Electrochemical Applications of in Situ Scanning Probe Microscopy

ARTICLE *in* CHEMICAL REVIEWS · JULY 1997

Impact Factor: 46.57 · DOI: 10.1021/cr960067y · Source: PubMed

2 AUTHORS, INCLUDING:

Andrew A Gewirth
University of Illinois, Urbana-Champaign
207 PUBLICATIONS **5,508** CITATIONS

SEE PROFILE

Electrochemical Applications of *in Situ* Scanning Probe Microscopy

Andrew A. Gewirth* and Brian K. Niece

Department of Chemistry, University of Illinois, 600 South Mathews Avenue, Urbana, Illinois 61801

Received February 17, 1997 (Revised Manuscript Received April 15, 1997)

Contents

I. Introduction

The application of the scanning tunneling microscope (STM) and the atomic force microscope (AFM) to structural problems at the electrified solid−liquid interface is one of the most important advances in electrochemistry over the past decade. These techniques, known collectively as scanning probe microscopy (SPM), are important because they provide a hitherto unobtainable level of structural insight into surfaces in solution. Because the charge transfer or capacitive charging event central to electrochemical reactivity occurs within a few atomic diameters of the electrode surface in the inner Helmholtz plane, the detailed arrangement of atoms and molecules at this interface strongly controls the corresponding electrochemical reactivity. Indeed, one of the principle goals in almost every area of chemistry is to correlate structure with physical properties. The focus of this review is to describe recent advances (ca. 1991 to the end of 1996) in *in situ* electrochemical STM and AFM imaging directed toward understanding processes at the solid/liquid interface.

Prior to the development of the scanning probe microscopies, structural information about the electrode surface either had to be inferred from the results of spectroscopic or electrochemical measurements, or elucidated using what are known as "*ex situ*" methods wherein the electrode is removed from solution and transferred into the ultrahigh vacuum (UHV) environment.[1] The *ex situ* method of examination has a long and illustrious history, despite the inevitable problems associated with the removal of the electrode from solution. Another, related method of electrode examination is the "*non-situ*" method wherein a metal surface is prepared in UHV and then subsequently dosed with water at low temperatures and possibly various cations or anions in order to simulate the electrode surface and its constituents.[2] This constructed interface is then examined using the techniques of vacuum surface science. Both of these methods have yielded considerable insight into electrode structure and dynamics. However, even their strongest supporters would concede the necessity of obtaining information from the real electrode surface, in solution and under potential control. The SPM techniques are among the few that can offer this perspective.

Sonnenfeld and Hansma[3] were the first to use the STM to study a surface immersed in a liquid. Their

* Author to whom correspondence should be addressed.

S0009-2665(96)00067-2 CCC: $28.00

Andrew A. Gewirth was born in Chicago in 1959. He received an A.B. in chemistry from Princeton University in 1981 and a Ph.D in 1987 from Stanford University where he studied physical bioinorganic chemistry under the direction of Professor E. I. Solomon. He was a postdoctoral fellow at the University of Texas at Austin in 1987–88 with Professor A. J. Bard where he worked on developing electrochemical applications of the scanning tunneling microscope. In 1988 he joined the Chemistry Department at the University of Illinois where he is now an Associate Professor. His research interests include surface electrochemistry, monolayers and multilayers at surfaces, deposition and corrosion, and interfacial phenomena.

Brian K. Niece was born in Michigan in 1970. He received his B.S. in chemistry from the Georgia Institute of Technology in 1992. He is currently a Ph.D. candidate in inorganic chemistry working under the direction of Professor Andrew A. Gewirth at the University of Illinois at Urbana-Champaign. His thesis research focuses on the binding of metal adatoms and molecular adsorbates to electrode surfaces. In the fall of 1997, he will join the faculty of Assumption College in Worcester, MA, as an Assistant Professor of Chemistry. His research interests involve the study of improved electrode materials for storage batteries and catalytic fuel cells.

images of highly oriented pyrolytic graphite (HOPG) in solution created a great deal of excitement in the electrochemical community, and it was only a short time before other images—although at much lower resolution—in redox-active solution were obtained.[4] Following these initial efforts in 1986, a rapid series of advances yielded high-resolution images of steps and terraces,[5−7] graphite atoms,[8] halide adsorbates on surfaces,[9] and, finally, metal atoms on surfaces,[10] these last three all obtained in solution and under potential control.

Development of *in situ* electrochemical SPM was dependent on three advances. First, of course, was the development of the STM and AFM instrumentation. The initial work by Binnig and Rohrer[11] in developing the STM had far reaching consequences in many areas. These techniques have had great impact on a large number of areas of interfacial science. A number of books and articles, including many in this issue, describe advances in the use of SPM to study surfaces and interfaces.[12−17]

The second advance is perhaps less well appreciated. Preparation of surfaces for work in UHV typically consists of a series of polishing steps outside the vacuum chamber followed by *in vacuo* steps consisting of ion sputtering and/or high temperature annealing. For surfaces that are to remain outside UHV, these processing steps are not available. This recognition led to considerable effort on the part of the electrochemical community to develop methods for metal electrode surface preparation. The most successful of these, developed initially by Clavilier[18] for Pt surfaces and later extended by Hamelin[19] for Au, utilizes high-temperature flame annealing followed by quenching in solution to give smooth, clean, contamination-free surfaces. At the present time, flame annealing methods exist for Au, Pt, Rh, Ir, and possibly some faces of Ag. Reductive annealing methods have also been developed for Ni. Cleaning and annealing procedures for all other metals remain somewhat less well-developed. These other metals, such as Fe, W, or Cu, readily form an oxide in the presence of oxygen, the absence of which is hard to ensure outside of UHV. Several layered materials, such as graphite and the dichalcogenides, can be prepared by cleaving, usually with tape, followed by rapid immersion of the cleaved surface. For semiconductors, chemical passivation of etched surfaces is the only way to prepare well-characterized planar materials under ambient conditions.

The third advance was the development of methods to actually perform the SPM experiment *in situ*. For STM, the crucial steps were to develop methods and materials with which to coat the STM tip and to couple the STM with a bipotentiostat. The faradaic background from a bare metal wire immersed in solution can approach several milliamps of current while tunneling currents are typically on the order of nanoamps. A consequence of this fact is that the STM tip must be insulated by coating all but its very end with an insulator so that the tunneling current will not be overcome by the electrochemical background. Materials successfully used to coat tips include nail polish, polyethylene and other polymers, varnish, glass, and wax.

The AFM[20] requires less modification than STM to operate with the sample in the electrochemical environment. An external potentiostat suffices to provide potential control, and no additional precautions are required to submerge the sample in electrolyte and image successfully. Indeed, the initial efforts examining metal surfaces in solution[21] were followed closely by electrochemical work.[22]

There are a number of reviews of electrochemical applications of probe microscopy. Early reviews include those by Hill et al.,[23] Arvia,[24] Kolb et al.,[25] Siegenthaler and Christoph,[26] Christensen,[27] and Sonnenfeld et al.[28] One of the most comprehensive of these is by Siegenthaler,[29] who described instrumentation, tip coating methods, and experimental results up until mid-1991. Siegenthaler's review is an excellent report of early work utilizing STM to

examine electrode surfaces. However, the year of Siegenthaler's review was really the first year that atomic resolution images on metal surfaces were obtained in solution by both STM and AFM and the intervening years have seen considerable growth in the area. Some of this growth is reflected in reviews by Weaver,[30,31] Bard et al.,[32] and a NATO Advanced Study Institute volume.[33]

Other techniques also provide high-resolution structural information from the solid−liquid interface. The development of *in situ* SPM methods has been nearly coincident with the extension of the surface X-ray scattering (SXS) methodology to study surfaces immersed in solution.[34−37] While both SPM and SXS provide information about surface structure, the techniques are highly complementary. SXS provides higher resolution than SPM, but the information is the result of an areal average. Furthermore, SPM can image lighter atoms and molecules on the surface which do not scatter X-rays well; however, SPM is relatively insensitive to atomic or molecular identity. X-ray reflectivity can also provide insight into structure normal to the electrode surface. As with other areas, a combination of techniques can often provide superior insight into a physical problem.

In this review we describe the results of *in situ* investigations of electrode surfaces using SPM. Topics include the structure of bare metal surfaces, monolayers and multilayers of metals formed atop them, semiconductors, and adsorbates.

II. Bare and Oxide-Covered Surfaces

When the STM was first applied to *in situ* studies of electrochemical interfaces in about 1988, much work focused on studies of metal electrodes and their surface changes in the double-layer potential region. The noble metals Au, Pt, Pd, and Rh, have been extensively studied and their surface features compared with those observed in vacuum. Similar studies have been performed on the more reactive metals Ag, Cu, and Ni, as well as on glassy carbon. Further studies have probed the surface changes engendered by the formation of surface oxides on many of these metals. These studies will be discussed in this section.

A. Gold

The first efforts examining bare Au surfaces in solution looked at large-scale changes under applied potential. The Kolb group first imaged the gold surface *in situ* with the STM.[5] They observed atomically flat terraces measuring several hundred angstroms across on Au(111). They did not attain atomic resolution on these terraces. However, 2.5 Å high steps were observed which correspond to monatomic steps. Following addition of Cl^- the authors obtained images that appeared noisy at positive potentials where the Cl^- is adsorbed to the electrode. Upon returning the electrode to more negative potentials where the Cl^- desorbs, they found that the topography of the surface had been altered significantly. Steps were observed to have grown in some areas while pits had formed in others to provide the material for step growth. This indicates that gold atoms are highly mobile following Cl^- adsorption. Later, Morita et al. also studied Au(111) electrodes in the presence of Cl^-.[38] They observed a similar roughening of the surface in the Cl^- adsorption region. They also reported the formation of bumps on the surface at lower potentials which they attributed to reduction of Au complexes formed with the Cl^- at higher potentials.

Trevor et al. studied the Au(111) surface during and after potential excursions as far positive as gold oxide formation.[39] They found that cycling the potential to a value where a single monolayer of Au oxide formed resulted in little change in surface topography. Cycling to higher potentials, where greater than a single layer of oxide formed, however, left the surface covered with pits of 40 Å or less in diameter and one monolayer deep. Allowing the electrode to sit at potentials where the oxide is reduced caused the surface to anneal, and the pits to merge with step edges and disappear. Excursions to even more positive potentials resulted in similar behavior with larger pits and longer times required for the surface to return to its original state. The addition of chloride caused an increase of the surface mobility as was observed by Kolb and co-workers, thus, the surface roughening could not be observed. This paper was noteworthy because it confirmed inferences about changes in the structure of Au(111) following oxidation made from voltammetric data. This was the first real correlation of electrode surface structure discerned by *in situ* STM with voltammetry.

Gao et al. studied the oxide formation process on Au(111) more extensively with STM.[40] In the potential region where gold oxide was present on the surface, they initially observed roughening as the oxide began to form. As the oxide formation progressed, the surface appeared less rough, but disordered laterally, even though atomic resolution in the $x-y$ plane was routinely observed by this time. Upon cycling the potential back to a region where the oxide is reduced, they also observed the formation of pits on the surface. Translating the imaged area to include regions which had not been scanned during the oxide formation and reduction, however, revealed that the pits where much smaller in the regions where the tip had not been scanning. This indicates that the presence of the tip may play a role in the formation of these pits during the oxide formation.

Nichols et al. studied the surface behavior of Au(100).[41] They found that in H_2SO_4 solution, the electrode surface was initially covered with small islands. These islands were asserted to have been formed from the extra material which is released when the surface reconstruction is lifted upon immersion of the electrode as will be discussed below. These islands were stable at low potentials, but cycling to higher potentials within the double-layer region led to the movement and eventual disappearance of the islands. When the potential was held at high potentials for a long time additional surface mobility was observed, including the straightening of step edges. As on Au(111), they observed that the mobility of Au surface features was enhanced in the presence of Cl^-. Finally, they observed that the formation of Au oxide at positive potentials resulted

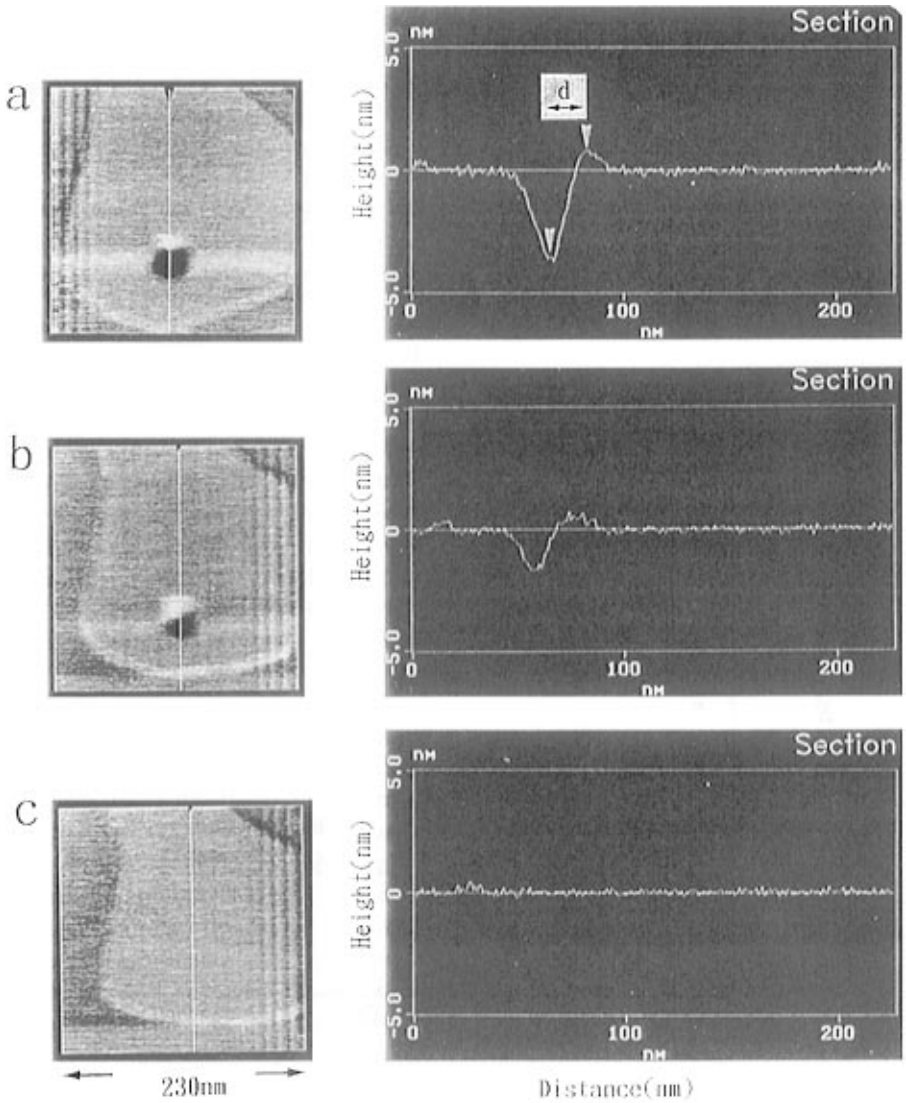

Figure 1. Set of AFM images (230 nm × 230 nm) together with cross-section profiles obtained at 980 mV showing the refilling process of the hole created on the terrace. Image a was taken immediately after creating the hole. The subsequent images were obtained 51 s (b) and 89 s (c) after image a. (Reprinted with permission from ref 44. Copyright 1995 Elsevier Science.)

in images of a rough surface, followed by the formation of pits which annealed over time, as was seen on Au(111).

Batina et al. used the STM to correlate the initial surface structure of Au(100) electrodes after different methods of pretreatment.[42] They found that if the electrode was quenched rapidly after flame annealing, the surface appeared very rough, albeit unreconstructed. As was earlier determined, however, holding the electrode at a more positive potential allowed the surface to anneal and develop atomically flat terraces. Breuer et al. also studied the effect of pretreatment of Au electrodes on the surface state.[43] They observed that flame annealing of polycrystalline gold foil to the point where it almost melts resulted in facets with primarily 90° angles between the edges. This suggests that the surface has formed terraces with (100) texture. In addition they achieved atomic resolution on the terraces, and observed that the foil reconstructs in the same manner as Au(100) single crystal surfaces, as discussed below.

Ikemiya et al. used the AFM to perform a quantitative analysis of the diffusion coefficient of Au(100) under potential control.[44] They scanned a small area of the surface at high force until a five atomic layer deep pit had been dug. They then reduced the tip force on the surface and imaged a larger area including the pit until the pit had filled back in, as shown in Figure 1. The holes were completely refilled in times on the order of several minutes. They found that the highest values of the diffusion coefficient in the double-layer region occurred at the highest potentials, as was previously observed qualitatively. The coefficient decreased to a minimum at the pzc, and increased again at more negative potentials. They ascribed this variation to the fact that interactions between Au atoms and charged or polar solution species increase as the potential moves away from the pzc, and also to changes in the excess charge density affecting the Au−Au bonds at potentials other than the pzc.

B. Platinum

Itaya and co-workers studied Pt electrodes by *in situ* STM as early as 1988.[45] They observed that polycrystalline electrodes were initially flat, but that

repeated (~50) cycles to oxidizing potentials resulted in surface roughening, as is also the case on Au surfaces. On the unroughened surface they observed atomically flat terraces and steps with heights of a few monolayers (1−10 Å). They observed both parallel ridges separated by about 150 Å, and domelike structures with diameters of about 50 Å. Uosaki et al. observed similar roughening effects after oxidizing the Pt surface and stepping the electrode back to negative potentials.[46] They studied the formation of both the parallel ridges and domelike structures over a period of minutes after the potential steps. Szklarczyk et al. observed the surface by STM imaging in the oxide formation potential region.[47] They observed that the surface was considerably roughened in this potential region, but then smoothed out again upon reduction. If the oxidation was performed at sufficiently high potentials, however, the original surface topography was never reobtained.

More recently, Sashikata et al. studied the oxidation of single crystalline Pt(111) by *in situ* STM, and were able to obtain a more detailed picture of the oxide-induced surface roughening.[48] They observed initially atomically flat terraces separated by monatomic steps. After a single oxidation cycle, the electrode exhibited single atom and small cluster defect islands. After five cycles, the surface reached a "steady-state" roughness which did not change with further potential cycling, as shown in Figure 2. This roughness was characterized by the presence of 2−3 nm diameter islands of 0.50−0.75 nm height (2−3 atomic layers).

Vogel et al. characterized the surface state of the low-index faces of Pt protected by I atoms in the electrochemical environment.[49] On the (111) and (100) faces, they found atomically flat terraces of several hundred nanometers in size, separated by the ubiquitous monatomic steps. On the Pt(100) surface, the step edges were clearly observed to form 90° angles with each other in keeping with the crystallographic symmetry of the electrode face. On the (110) face they observed parallel ridges, reminiscent of those seen on formerly oxidized polycrystalline electrodes. On Pt(332) electrodes, they observed that the surface became faceted with large steps and narrow terraces. Delaying the addition of I to the surface until the crystal was cool allowed them to obtain near atomic resolution images of the surface.

C. Rhodium

In addition to their work on Pt, Sashikata et al. also studied the roughening of Rh(111) after electrochemical oxidation with the STM.[48] They found that after a few potential cycles a steady-state roughening was reached as was the case in the platinum system. The features observed were similar in size to the bumps formed on Pt(111). The roughness appeared to be much less ordered, however. This group later reported a method of preparing atomically flat Rh(111) which does not involve cooling in I_2 vapor.[50] Their crystals were flame annealed, cooled in a hydrogen atmosphere, quenched in H_2-saturated water, and then immersed in KI solution before being characterized with the STM. This characterization revealed atomically flat terraces, and roughening upon potential cycling similar to that observed earlier.

D. Palladium

In contrast to the rhodium and platinum systems, Sashikata et al. observed considerable roughening on Pd(111) electrodes following oxidative potential cycling.[48] STM images revealed that the surface was not quite as smooth as Pt(111) and Rh(111) electrodes upon initial immersion. A few potential cycles yielded a steady-state roughness that exhibited a much larger corrugation than on the other two metals. The roughness was disordered, like that on Rh(111), and the islands were 2−3 nm tall. They attribute this difference to a roughening mechanism which involves dissolution and redeposition of Pd metal, whereas the Pt and Rh oxidation reactions involve only place exchange in the formation of an oxide layer.

More recently, Soriaga, Itaya, and co-workers have also studied the dissolution of Pd electrodes with *in situ* STM.[51] They observed that the presence of an I^- monolayer on the electrode surface enhances the oxidative dissolution of step edges. Prolonged dissolution of step edges results in surface smoothing.

E. Silver

Morita et al. first examined the surface structures of polycrystalline Ag electrodes in Cl^- containing electrolyte with the STM in 1989.[38] They found that when the potential was changed from a positive to a negative value that the surface appeared more rough. They attribute this change to reduction of the AgCl adlayer formed at high potentials. They found at even more cathodic potentials that the surface roughness began to decrease. They attribute this change to rearrangement of the Ag surface atoms as Cl^- adatoms are desorbed from the surface.

Christoph et al. studied Ag(100) surfaces in chloride-free electrolyte at about the same time.[52] Under these conditions, they found terraces of 5−20 nm in width separated by monatomic steps. Between these terraces were areas covered with domelike structures. Höpfner et al. later presented a method of preparing electrochemically grown quasi-perfect Ag(100) faces which they characterized *in situ* with the STM.[53] They observed similar terraces to those seen by Christoph on Ag(100) single crystals. Using microelectrodes grown electrolytically in Teflon capillaries, they observed atomically flat terraces of much larger extent (several hundred nanometers) separated by monatomic steps. In the same study they observed the motion of steps across the surface over time on the quasi-Ag(100) surfaces.

Kolb's group performed a more detailed analysis of the dynamics of monatomic steps on Ag(111) single crystal electrodes.[54] They attributed "frizziness" seen in STM images at step edges to the diffusion of kink defects along the step edge. They noted that such frizziness was not seen at screw dislocations until far enough from the defect that the step edge was at least monatomically high. They also observed that the extent of the frizziness increased with increasingly positive potentials until it was 2−3 atomic diameters deep, indicating the diffusion of multiatomic kink

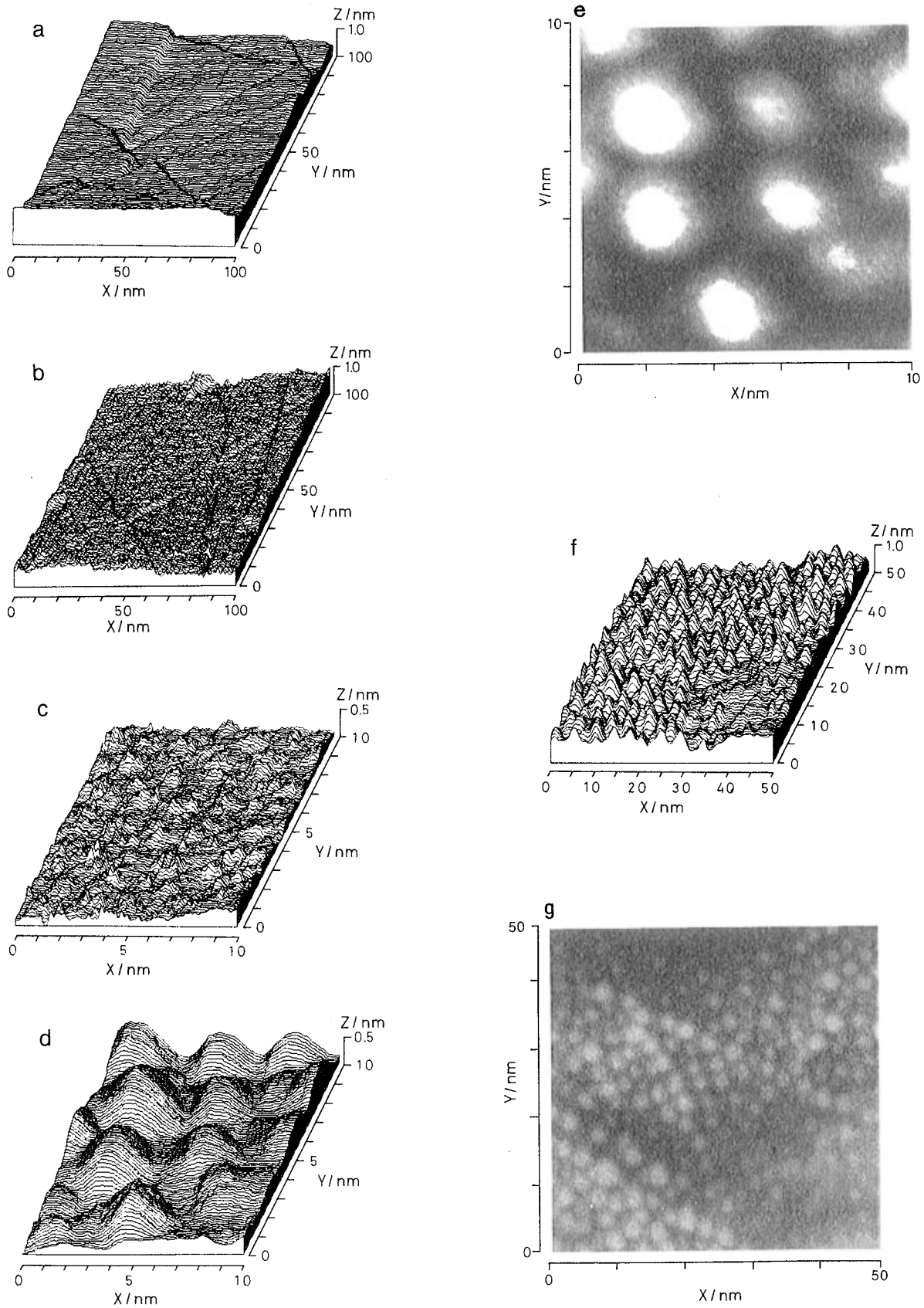

Figure 2. STM images acquired on a Pt(111) facet in a 0.05 M H_2SO_4 solution before (a) and after 1 (b) and (c) and 10 (d,e,f, and g) potential cycles. Gray-scale images e and g are top views of d and f, respectively. The electrode potentials of the Pt(111) and tip electrodes were 0.8 and 0.85 V vs RHE, respectively. The tunneling current was 1 nA. The *x*, *y*, and *z* scales are as indicated. (Reprinted with permission from ref 48. Copyright 1991 American Vacuum Society.)

sites. They estimated the diffusion rate of the kink sites along the step edges to be at least 3000 nm/s. Diffusion of defects at step edges on Ag has also been observed in UHV,[55−57] and the defect mobility in this case scales with temperature—the UHV analog to applied potential.

F. Copper

While methods to prepare surfaces of Ag, Au, and Pt are well developed, such is not the case with more reactive materials such as Cu. This lack is unfortunate, as Cu is important in applications as diverse as electronics, deposition, and catalysis. The first efforts directed toward the study of Cu surfaces thus interrogated their structure and reactivity.

Examination of Cu(100) surfaces prepared by electropolishing revealed a $(\sqrt{2}\times\sqrt{2})$R45° structure instead of the expected (1×1) lattice.[58] One of the problems with the probe microscopy is the lack of direct chemical identification of species imaged. There are three possibilities as to the identity of the adlattice: anions from solution, chloride present as an impurity, or oxygen or hydroxide present as a monolayer. Insensitivity of the structure to anion excluded the first possibility. On Cu(111), only a diffuse overlayer was observed, different from the $(\sqrt{3}\times\sqrt{3})$R30° adlattice found in the presence of Cl^-.[59] On Cu(110) crystals during the initial stages of oxidation they found (100) oriented chains, arranged primarily in (2×1) and (3×1) patterns grew in following excursion to rest potential from very negative potentials. [60] Addition of Cl^- to this system resulted in a completely different structure, strongly suggesting that the observed overlayers were indeed formed by an oxygen or hydroxide adlattice.

Ikemiya used the AFM to characterize the native oxide films formed on Cu(111) and Cu(100) electrodes in alkaline solution.[61] He observed atomically flat terraces and monatomic steps as has been seen on other metals. Atomic resolution images at negative potentials revealed the Cu(111) and Cu(100)-(1×1) bulk structures. At more positive potentials where the surface is believed to exist as Cu_2O, structures were observed which retained the symmetry of the bulk metal but had a more open spacing (0.60 nm and 0.43 nm on (111) and (100), respectively vs 0.26 nm for bare Cu). They assigned this structure to the O atoms in the truncated Cu_2O lattice. The Cu_2O surface was observed to be highly stepped, as shown in Figure 3. The increase in step density was believed to arise from release of the strain induced by the slight lattice mismatch between the metallic Cu and Cu_2O structures.

G. Nickel

Early STM studies of Ni foil electrodes by Lev et al. revealed flat terraces.[62] Measurement of the tunneling current while the tip−sample separation was varied indicated the expected response at the rest potential and in the dissolution potential region, wherein the current rises to a sharp peak as the tip approaches the surface and decays quickly as the tip is retracted. In the passive potential region, however, the current decay is asymmetrical and does not decay immediately when the tip is retracted. This response was attributed to the resistive nature of the oxide layer present on the surface in this region.

Scherson and co-workers have studied the surface structures of nickel hydrous oxide films—such as those used in Ni−Cd batteries—after repeated potential cycles.[63] They found that the initial oxidation

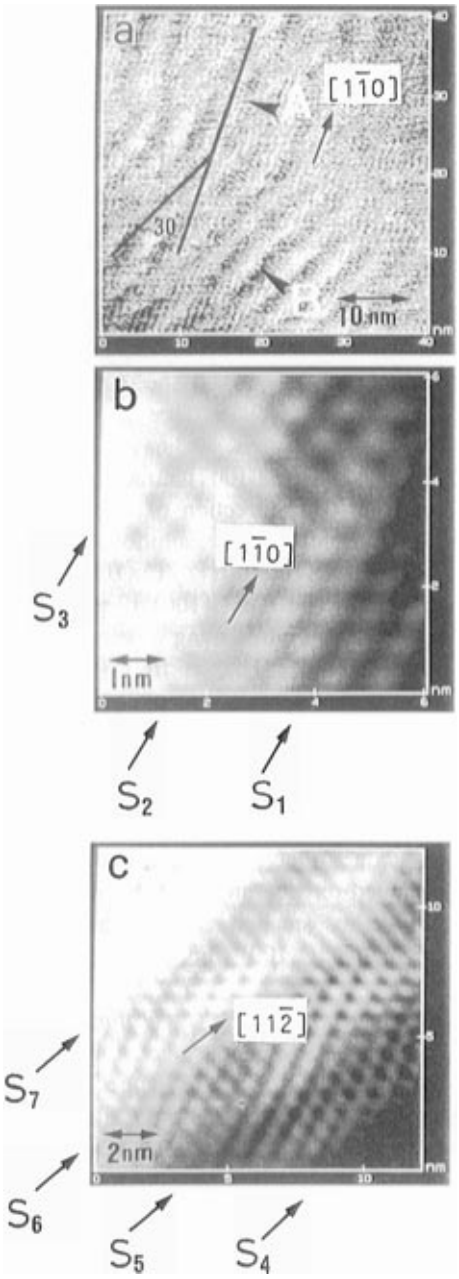

Figure 3. Unfiltered and top-view AFM images of stepped surfaces of a Cu_2O(111) film in 0.1 M NaOH solution obtained at −0.12 V (a). High-resolution images of locally faceted step edges marked A (b) and B (c) (filtered data). The [1$\bar{1}$0] and [11$\bar{2}$] directions of the bare Cu(111) surface are indicated by arrows. (Reprinted with permission from ref 61. Copyright 1995 Elsevier Science.)

cycle of the film from $Ni(OH)_2$ to NiOOH produced large crevices in the surface as shown in Figure 4. Subsequent reduction of the surface indicated that hairline fractures remained where the crevices had been. Future potential cycles reveal that the crevices always return at the same locations. The crevice formation is believed to occur because of the different densities of the Ni(II) (2.5−2.8 g/cm^2) and Ni(III) (4.7 g/cm^2) materials. The presence of the hairline fractures in the reduced material after initial oxidation indicates that the surface never truly heals from the stress caused by the oxidation, and provides insight into the mechanism of capacity loss and eventual failure in nickel oxide electrodes.

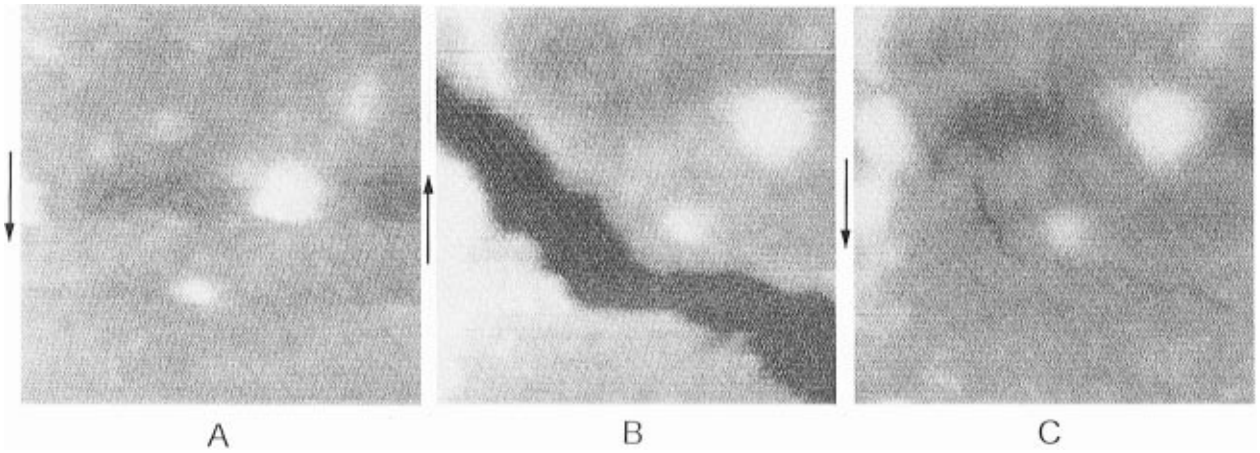

Figure 4. *In situ* AFM images of a 0.1 μm × 0.1 μm area of a $Ni(OH)_2$(hyd) film (ca. 3.2 mC) supported on HOPG(bp) obtained at a potential of 0.15 V vs SCE, i.e. fully reduced state, in 1.0 M KOH in the *fluid cell* after transfer from the preparation cell (frame A). Frames B and C were obtained at 0.33 and 0.015 V in the same area after stepping the potential twice between these two values. The arrow on the left side of the pictures indicates the direction of the AFM *vertical* scan. (Reprinted with permission from ref 63. Copyright 1994 American Chemical Society.)

High-resolution work performed more recently by Suzuki et al. has revealed the oxide layers on Ni single crystal electrodes.[64] At cathodic potentials on Ni(111) they were able to observe the expected (1×1) hexagonal lattice. At more anodic potentials, they observed hexagonal oxide overlayers. On Ni(100), they observed a p(2×2) oxygen layer at cathodic potentials, and a quasi-hexagonal structure at more anodic potentials which they attributed to the formation of bulk oxide. This work was noteworthy because it showed that reductive annealing methodology could prepare suitably smooth Ni surfaces.

III. Reconstructions and Restructurings

It has long been known that metal surfaces in vacuum reconstruct in order to minimize their surface energy. The extent of a reconstruction is often strongly dependent on the work function of the metal being studied, and studies of the reconstructed surface can provide information about the charge density and distribution on the surface. The electrochemical environment offers a unique opportunity to systematically vary the electronic state of a surface, both through application of a potential and the influence of adsorbed species in solution. Kolb has written an extensive review of the current state of knowledge about reconstructions in electrochemical systems.[65] The ability of the scanning probe techniques to provide real-space structural information about the state of the surface as the conditions are varied has yielded a wealth of new information about the reconstruction of metal surfaces—especially those of gold electrodes.

A. Gold

When prepared by the flame annealing technique, the low-index faces of gold are all known to exhibit reconstructions which can be removed electrochemically by placing the electrode at a sufficiently positive potential.[66] Kolb and co-workers determined that the Au(100), (111), and (110) surfaces exhibit (5×20), (1×23), and (1×2) reconstructions, respectively, by placing the electrodes in vacuum and studying them by RHEED. The removal of the reconstruction was later attributed to adsorption of electrolyte anions at higher potentials. Hamelin observed electrochemically that the Au(100) reconstruction could be reformed electrochemically by holding the electrode at negative potentials for an extended period of time.[67]

Weaver's group has investigated the potential induced reconstruction of Au(100) in depth with the STM, and were able to image the formation of the reconstructed structure.[68−71] A similar structure has been seen by Magnussen et al.[72] At high potentials, they observed the expected square Au(100) (1×1) surface lattice. At lower potentials, however, they observed the formation of rows of gold atoms which are staggered to form a quasi-hexagonal pattern, and compressed so that six atomic rows fit into 14.5 ± 0.5 Å (five Au interatomic spacings).[68] They assigned this structure as a (1×5) reconstruction and associated it with the "hex" reconstruction observed in vacuum. They observed that several different height modulations of the rows could be seen depending on the registry of the topmost layer of atoms with the second layer (a moiré pattern). They also observed that the reconstruction was not initiated until potentials significantly below those where electrolyte (in this case ClO_4^-) adsorption begins, thus ruling out the possibility that the reconstruction is lifted by specific adsorption of anions.

In further studies, this group observed that the Au(100) surface is essentially unreconstructed after flame annealing and cooling in ultrapure water.[69] The reconstruction can then be formed by sweeping the potential to negative values and holding. In addition, they later assigned the reconstructed structure to a (5×27) lattice which is compressed in both substrate lattice directions. Longer range observations of the reconstructed surface revealed that there are domains which retain more of the Au(100) texture, rather than being fully reconstructed to the quasi-hexagonal structure.[70] These variations in surface structure, and hence surface charge density, were used to explain the broadening of the capacitance well observed at the pzc on the reconstructed surface,

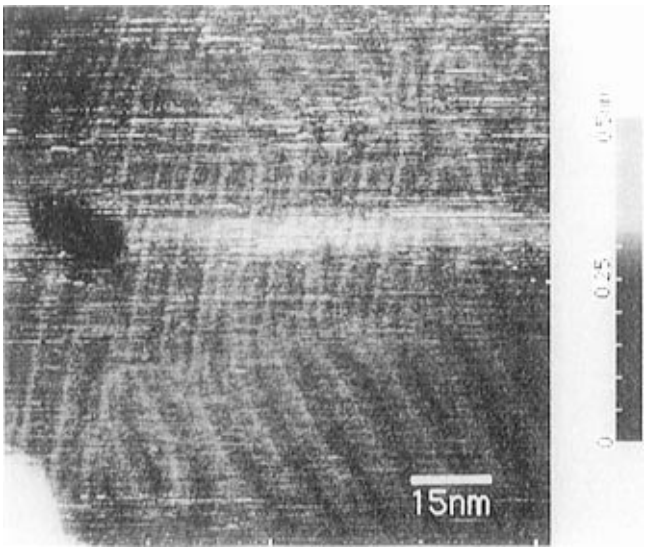

Figure 5. Image of Au(111) under 0.1 M $HClO_4$ solution. A transition from the ($22 \times \sqrt{3}$) stripes at the upper $^2/_3$ of the frame to abnormal stripes at the bottom of frame is shown. (Reprinted with permission from ref 73. Copyright 1991 American Institute of Physics.)

as the pzc would have different values in the different domains.

A compressed reconstruction at negative potentials on Au(111) has also been observed by Tao and Lindsay,[73] as well as the Weaver[74] group. They designate this structure as ($\sqrt{3}\times22$) which is essentially the same as the (1×23) symmetry observed *ex situ* by LEED. This reconstruction involves a shift from fcc to hcp stacking, and a compression of the Au lattice in the ($1\bar{1}0$) direction so that 23 atoms fit into the space of 22 atoms in the bulk. This reconstruction results in the appearance of waves on the surface as the reconstruction goes in and out of registry with the underlying Au lattice. Longer range images, like that seen in Figure 5 show that these waves form paired rows which periodically make turns at multiples of 60° which has led to the naming of this structure as the "herringbone" reconstruction. Cycling the potential to a region where the reconstruction is removed and then back reveals changes in the shape of the step edges on the surface, indicating that the extra material required in the compressed structure is taken from and returns to the step edges.

More recently, Weaver and co-workers undertook a systematic study of the reconstructions of the (110) and several high-index faces of Au in the electrochemical environment to compare with the understanding developed for the other low-index faces of this metal.[75] Au(110) electrodes were observed to reconstruct into the missing-row structures observed in UHV at low potentials. The images revealed (1×2) and (1×3), as well as more open ($1\times n$) regions. The average atomic density of the reconstruction was believed to be approximately that for the (1×3) structure. Like the other low-index faces, the Au(110) surface was observed to not be reconstructed at potentials above the pzc. Magnussen et al. have observed similar structures on the Au(110) surface.[76]

The high-index faces chosen for this work were arranged between the low-index faces along the stereographic triangle, and all had steps and terraces consisting of the low-index faces for comparison. At low potentials, the Au(331) face, which can also be denoted 3(111)-(111) in step-terrace notation, was observed to undergo a (1×2) reconstruction resulting in paired rows. They proposed a model where every other terrace edge atom moves one atomic spacing to pair with another terrace edge atom. At higher potentials, they observed a relaxation of the surface, where the terrace edge atoms move down slightly, resulting in a less deep corrugation of the surface. The Au(221) face, 4(111)-(111), exhibits a similar relaxation, but no reconstruction is observed at lower potentials. This is believed to be because the one atom wider terraces prevent movement of terrace edge atoms to pair with each other.

At low potentials, the Au(311) and (533) faces—2(111)-(100) and 4(111)-(100), respectively—both exhibit a terrace edge relaxation like that seen on the (331) and (221) faces. No reconstruction is ever observed, however. Finally, the very open Au(210) and (410)—2(110)-(100) and 4(110)-(100), respectively—show no reconstruction or clear relaxation. The surface exhibits atomic level order in the $x-y$ plane, but there are no large flat domains. Instead, from long range, the surface appears disordered in the z direction.

Surface structural changes and deformations can be induced by the presence or absence of adsorbates, in addition to being induced by surface charge changes. Haiss and Sass have observed long-range deformations of the Au(111) surface during the underpotential deposition of Cu.[77] They used an STM to measure the vertical movement of the electrode during deposition, and found that at high potentials, the adsorption of sulfate caused a compressive stress (and corresponding increase in the surface height). The coadsorption of Cu and sulfate in the intermediate region resulted in little surface stress, but at sufficiently low potentials, the surface is again subject to compressive stress caused by residual sulfate on top of a complete layer of neutral copper adatoms.

The Au(100) potential-induced reconstruction is well understood, and has also been studied in the presence of specifically adsorbed molecules. In basic solution, Edens et al. found using the STM that the Au(100) quasi-hexagonal reconstruction formed much as it does in acidic solution.[78] They also observed the growth of pits during the formation of the reconstruction, which presumably supplied the extra Au atoms necessary to complete the reconstructed layer. Upon cycling to positive potentials where the reconstruction is lifted, the excess material did not fill in the pits, but formed small (1×1) clusters on top of the originally flat terraces. The higher concentration of OH^- seems to enhance the mobility of the Au atoms during potential cycling. The introduction of CO into the solution allowed the reconstruction to form at more positive potentials. This is counter to the effect of most adsorbates, and is believed to be due to the fact that CO adsorption actually increases the work function of metal surfaces, and would consequently increase the surface charge density, thus facilitating

the formation of the reconstruction at less extreme applied potentials.

Gao et al. observed two different restructurings of the Au(110) surface in the presence of iodide anions. At high potentials, where iodide adsorbs to the surface in a (1×1) adlayer, the underlying gold terraces were observed to restructure from wide island-like terraces to narrow strips with widths of 25−40 Å, as shown in Figure 6.[79,80] This rearrangement was proposed to arise from increased electrostatic repulsions in the I^- adlayer which destabilize the interior terrace domains relative to the terrace edges.

At negative electrode potentials on Au(110) in KI electrolyte, the same (1×3) reconstruction is observed as in other electrolytes.[81] In the presence of CsI, however, two other distinct adlayers are observed prior to the formation of the (1×3) structure, allowing the mechanism of formation of the reconstruction to be studied. At intermediate potentials, the surface forms a "one-missing-row" structure in which every third row of Au atoms is removed. This extra material can be observed forming individual strings of atoms on top of the reconstruction. At more negative potentials, the surface forms the (1×2) missing-row reconstruction where more of the gold rows have been removed so that every other row is absent. Finally, the surface forms the (1×3) three-missing-row structure in which two rows of the top layer and one row of the second layer are removed for each top row which remains.

B. Platinum

Zei et al. have also reported observation of the reconstruction of Pt(100) in the electrochemical environment.[82] The surface was prepared by the flame-annealing technique, similarly to gold, which is known to result in a reconstructed surface in vacuum. The surface was then immersed in the electrolyte solution under potential control at a sufficiently negative potential so that specific adsorption of anions does not occur. A (5×20) hexagonal reconstruction was observed which matches that found in vacuum. The reconstruction was lifted by cycling to higher potentials and could not be re-formed by holding the electrode at negative potentials. Vogel et al. have also observed what they believe to be a (2×1) reconstruction on iodine-protected Pt(332).[49]

Pt(100) has been observed to undergo structural changes upon changing the adsorbed anion at the surface. Villegas et al. prepared Pt(100) surfaces by flame annealing and cooling in an inert gas/iodine atmosphere to protect the surface with iodine.[83] The electrode was then immersed in a solution containing CO, CN^-, S^{2-}, or I^-. The adsorbed iodide was replaced with an adlattice of the solution species, and the Pt surface restructured to form two atom high islands of 20−50 Å across covering 50% of the surface. The rearrangement is believed to occur by the migration of half of the top layer surface atoms onto the other half, forming the islands. The driving force for this restructuring is proposed to be the resulting increase in step edge sites where Pt−adsorbate bonds can form which are more favorable than Pt−Pt bonds.

IV. Ionic Adsorbates

Studies of the adsorption of atoms and small molecules to metal surfaces have traditionally played a fundamental part in the study of surface interactions. The halogens have been especially well studied in UHV systems and are usually easily imaged in the electrochemical environment. Because of their relatively high atomic number, the heavier halogens such as Br and I are also easily interrogated using X-ray scattering methods, and there has developed an important correlation between the X-ray and SPM techniques. The *in situ* electrochemical structural techniques allow direct correlation of surface structures with surface potential, and hence surface charge. These advances allow direct control of adsorption/desorption and potential-induced phase transitions and has provided much new information about the behavior of the inner Helmholtz plane.

A. Halides

Iodine exhibits the strongest adsorption of the halides to many metals in electrochemical systems. The strength of the metal−iodine interaction has led to its use as a passivating layer to protect Pt surfaces after flame annealing for transfer through the atmosphere. The adlayers thus formed in air were first imaged *ex situ* by Schardt and co-workers, who observed two different surface structures on Pt(111), a $(\sqrt{7}\times\sqrt{7})$R19.1° adlattice with surface coverage of 0.43 ML, and a (3×3) overlayer with a coverage of 0.44 ML.[84]

In situ, iodine adsorbates have been observed on Pt(111),[49] Pt(110),[85] and Pt(100).[83] Vogel et al. observed the (3×3) overlayer seen in air by Schardt on Pt(111) under electrochemical conditions.[49] Villegas et al. immersed an I-protected Pt(100) electrode in I^- containing solution, and imaged a paired row structure which they assigned as $c(\sqrt{2}\times5\sqrt{2})$R45° adlayer with a coverage of 0.6 ML.[83] This structure was also observed by Vogel et al.[49] Stepping to negative potentials resulted in replacement of that adlayer by a simple $(\sqrt{2}\times\sqrt{2})$R45° overlayer with a coverage of 0.5 ML. DeSimone et al. imaged Pt(110) in an electrochemical environment after flame annealing and exposure to iodine vapor during cooling. The iodine forms a (1×2) adlayer with I rows between every other Pt(110) row.[85] The coverage of this structure increased with increasing exposure time to the iodine vapor. Close-packed rows of Pt reminiscent of the (1×*n*) reconstruction were also observed to form on the surface.

In contrast, on Au(110), two different potential-dependent iodine structures have been observed.[80] Gao et al. imaged the rectangular bare Au(110) structure at negative potentials. At slightly more positive potentials they observed a nearly hexagonal overlayer with a spacing of 4.4 Å in one direction and 4.8 Å in the other two directions, and a coverage of 0.62 ML. The rows of this structure are oriented 26° from the Au(110) rows. This structure compresses slightly as the potential is raised, until the structure changes to a (3×2) structure which is aligned with the Au(110) rows and has a coverage of 0.67 ML.

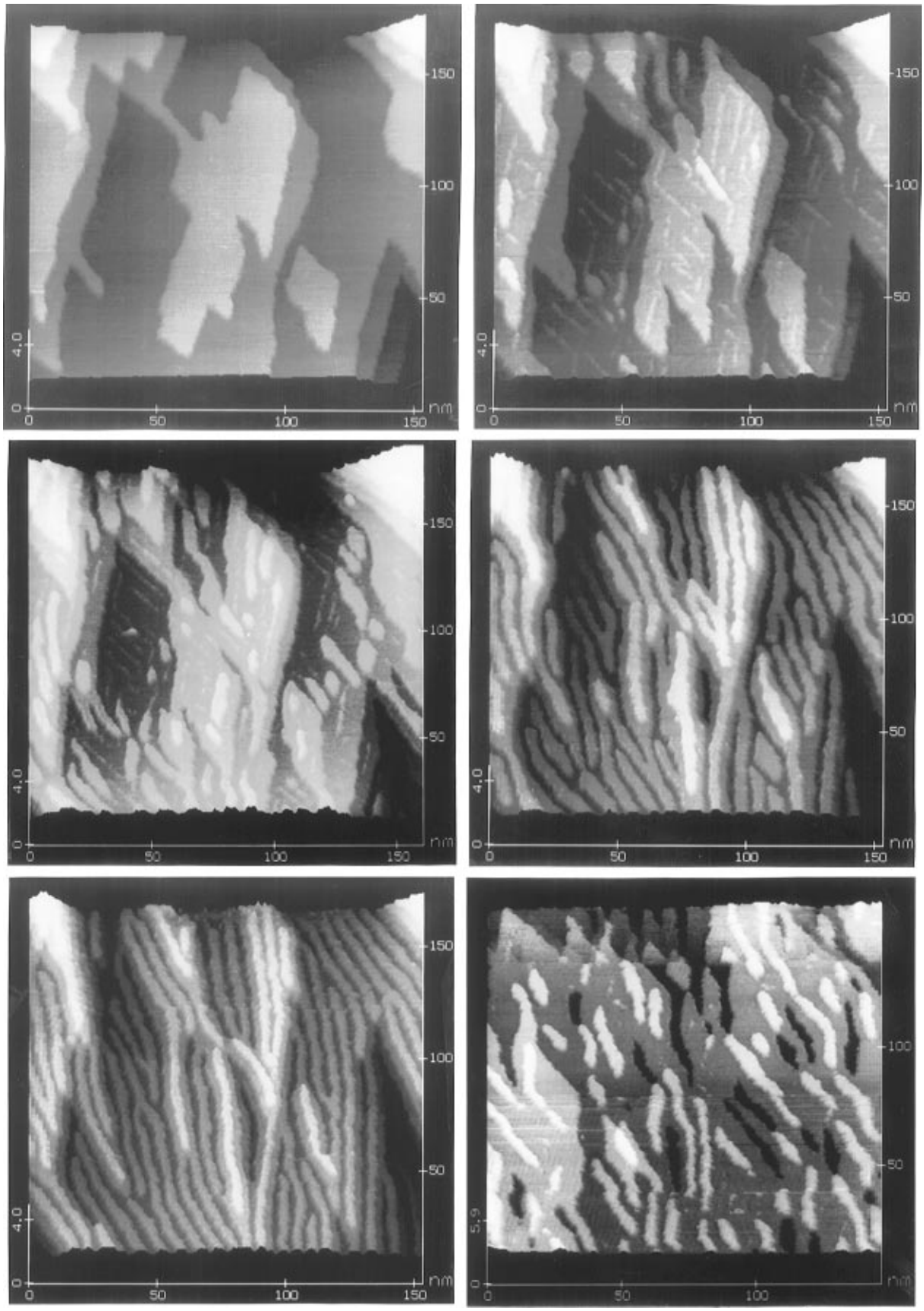

Figure 6. (a−e) Sequence of potential-dependent STM images for 150 nm square region of Au(110) in aqueous 5×10^{-3} M KI: (a, upper left) 0.1 V vs SCE; (b, upper right) 2 min after increasing potential to 0.25 V; (c, middle left) 2 min later, at 0.3 V; (d, middle right) 9 min later, at 0.35 V; (e, lower left) 3 min later, at 0.4 V; (f, lower right) largely single terrace surface region, 3 min after increasing from 0.2 to 0.32 V. Tip−substrate bias voltage ≅ −0.08 V; tunneling current ≅ 10 nA. (Reprinted with permission from ref 79. Copyright 1994 American Physical Society.)

Lowering of the potential resulted in stepwise reversal of the iodine adlayer formation, although the reverse processes occurred more slowly than the forward processes.

Tao and Lindsay found that iodine on Au(111) exhibited a ($\sqrt{3}\times\sqrt{3}$)R30° structure at low potentials, and a close-packed (3×3) structure at higher potentials.[86] A similar situation is observed by Yamada et al.[87−89] At low potentials, they report a rectangular c($p\times\sqrt{3}$)R30° overlayer which compresses from p = 3 to p = 2.49 as the potential is raised. The low coverage structure (p = 3) is observed to be identical to a ($\sqrt{3}\times\sqrt{3}$)R30° structure. At more positive potentials, the structure is observed to switch to a rotated hexagonal overlayer which is similar to the ($\sqrt{3}\times\sqrt{3}$)R30° overlayer with an additional 1−2° of rotation. This adlayer exhibited a moiré pattern due to the inequivalent binding sites of neighboring I adatoms, and also underwent electrocompression as the electrode potential was increased.

More recently, the Itaya group has characterized the influence of I adlayers on Pt and Au electrodes on the tunneling barrier height *in situ*.[90] They found that the barrier height was not significantly influenced by the electrode potential. The presence of the iodine adlayer, however, resulted in a significant decrease in the tunneling barrier relative to that found on the bare surface either in air or in vacuum.

Tao and Lindsay also report a ($\sqrt{3}\times\sqrt{3}$)R30° structure on Au(111) at low potentials in Br^- containing electrolyte.[86] At higher potentials they found a hexagonal close packed layer. The close packed structure was rotated by 20° from the underlying gold lattice, as they were able to determine by varying the tunneling parameters so that the hexagonal gold structure was seen. The behavior of Br^- on Pt(111) observed with the STM by Tanaka et al.[91] is similar to that observed on Ag by Sneddon and Gewirth. At potentials near the hydrogen evolution potential, they observed the bare Pt(111) lattice. At more positive potentials they were able to image ordered Br^- adlayers. In the double-layer charging region they imaged both symmetric and asymmetric (3×3) structures with a coverage of 0.44 ML. At potentials between hydrogen evolution and the formation of the (3×3) structure an incommensurate structure was observed.

The Ag−halide system is of special interest due to the adherent Ag−X layers which form during the initial stages of oxidation in the presence of the halides. Schott and White have studied the atomic-level structures formed by cooling flame-annealed Ag balls in aqueous HX solution by *ex situ* STM and scanning tunneling spectroscopy.[92−94] While not truly electrochemical, this work is an important starting point for electrochemical studies and will be discussed first.

They report that F and Cl form double-row structures on Ag(111) with coverages of 0.7 and 0.6 ML, respectively. Br forms a row structure with less pronounced row pairing and a coverage of 0.45 ML. I forms a distorted ($\sqrt{3}\times\sqrt{3}$) structure which has a coverage of 0.33 ML. They observed that the symmetry of the structures increased with increasing adsorbate size. They also observed that in mixed-halogen adlayers there was an increase in point defects, presumably due to the lattice mismatch between the two adlayer structures.[93] No equilibrium mixed structure was formed, but rather the more soluble anion was gradually replaced by the less soluble as the time in solution increased. Finally, they performed scanning tunneling spectroscopy studies of the adlayers and found a diode like response of the adlayer tunneling current to bias voltage.[94] The threshold voltage for the current response was correlated to the vibrational frequency of the various Ag−halide bonds.

Sneddon and Gewirth performed a similar study on Ag(111) films in an electrochemical cell with the AFM.[95] In F^- and Cl^- containing electrolyte they observed only the Ag(111) hexagonal lattice at potentials negative of silver oxidation. This correlates with Schott and White's observation that overlayers of the more strongly solvated halides bind to the surface weakly. In Br^--containing solution, a (3×3) adlattice was observed at potentials positive of the voltammetric wave which has been associated with the formation of ordered surface overlayers. Below this potential, only the bare Ag(111) surface was observed. The observed overlayer has a coverage of 44.5% which agrees with that observed *ex situ* by White in this region. In I^--containing electrolyte, they observe a ($\sqrt{3}\times\sqrt{3}$)R30° iodine overlayer. This structure also agrees with that reported by Schott and White. However, in the *in situ* work, comparison with images taken before I^- was added to solution allowed the adlattice orientation to be determined. This adlayer could not be removed from the surface at negative potentials.

Sneddon and Gewirth were also able to image the surface changes during Ag oxidation. In F^- and Cl^- solutions, only Ag dissolution was observed. In Br^--containing solutions AgBr protrusions were observed to form at step edges or defect sites. This is consistent with the fact that solid AgBr forms at potentials more negative than that required for AgCl formation. In I^- solution, AgI film formation was also observed. Roughening of the surface was observed in both of these systems upon reduction of the film, presumably due to displacement of Ag atoms during the halide adlayer formation.

B. Cyanide

Stuhlmann et al. observed the formation of ordered adlayers of CN^- on Pt(111) by *in situ* STM.[96] The observed structure, shown in Figure 7, has ($2\sqrt{3}\times2\sqrt{3}$)R30°-7CN symmetry. The overlayer consists of individual CN^- anions adsorbed in atop sites. Each of these is surrounded by six additional CN^- anions in near atop sites which are pushed out slightly from the central anion. Each such cluster is surrounded by a hexagon of Pt atoms with no adsorbed anions which separates the clusters. At lower potentials, this ordered structure gives way to a (2×2) structure and finally disordered adlayers.

The Itaya group has observed a structure with the same symmetry in solutions of CN^- on Pt(111).[97] They observed a variation in the intensity of the center spot of the structure with tunneling conditions, which they interpreted as a missing CN^- in the center of the hexagon. Bright spots were observed in the presence of K^+, however, which they attributed to cations complexed by the strongly adsorbed CN^-.

Sawaguchi et al. have studied the structures which form on Au(111) in the presence of $Au(CN)_2^-$ with

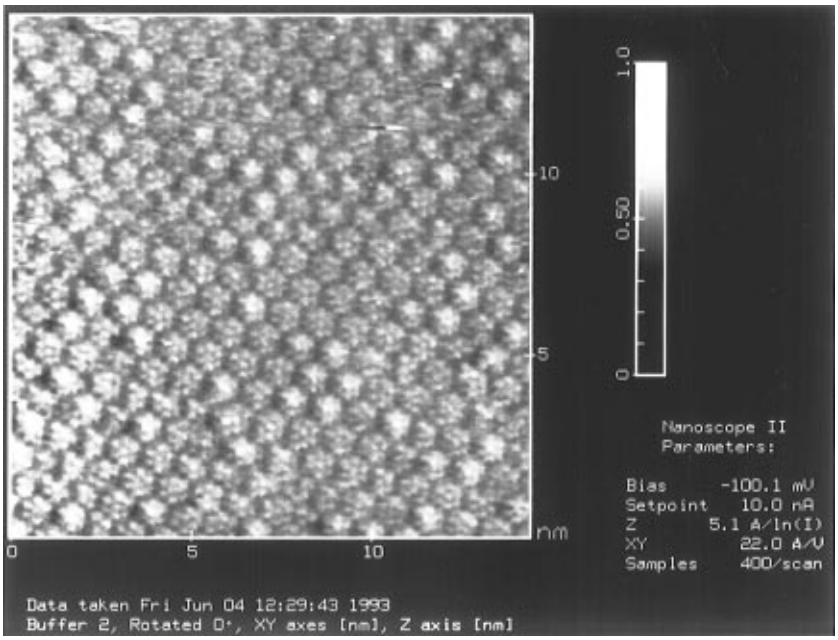

Figure 7. Typical mildly filtered STM image of a 5 nm square region of the $(2\sqrt{3} \times 2\sqrt{3})$R30°-7CN adlayer on Pt(111) in 0.1 M $NaClO_4$ (pH 10.5) at −0.4 V vs SCE. Substrate−tip bias potential = −100 mV; tunneling current = 10 nA. (Reprinted with permission from ref 96. Copyright 1994 Elsevier Science.)

the STM.[98] They observe two different structures on opposite sides of the reversible $Au(CN)_2^-$ redox peak. At potentials positive of the $Au(CN)_2^-$ redox peak they observe a p(1.15×√3)R30° structure with a coverage of 0.435 ML. At potentials negative of the peak, they observe a p(1.41×2√3)R30° structure with a coverage of only 0.355 ML. The overlayers in both regions are believed to be formed from $Au(CN)_2$ units which liberate a CN^- ion upon adsorption. The structures interconverted reversibly on potential cycling. The low coverage of the structure at more negative potentials is believed to arise from the incorporation of K^+ ions from the electrolyte into the adlattice to balance the residual CN^- charge after the Au is reduced.

C. Sulfide

Weaver and co-workers have investigated the behavior of sulfide on Au(111) electrodes using the STM.[99] At low electrode potentials, the S^{2-} anions were observed to form a (√3×√3)R30° overlayer on the Au surface. At more positive potentials where electrooxidation of S^{2-} to S begins, the formation of ring structures believed to consist of S_8 rings was observed. Finally, at the most anodic electrode potentials, the oxidized S^{2-} was observed to form an amorphous multilayer of sulfur. Itaya's group observed a c(2×2)-S adlattice on Ni(100) electrodes prepared by exposure to H_2S while cooling.[64]

D. Sulfate

Sulfate is an important anion in electrochemistry because its interaction with surfaces forms the basis of many early voltammetric studies. The direct observation of SO_4^{2-} adsorbed on a metal surface *in situ* with the STM was first reported by Magnussen et al.[100,101] They reported a (√3×√7) adlayer which was interpreted as consisting of rows of sulfate anions bound to the surface in a 2-fold symmetric orientation, as shown in Figure 8. Their model had a coverage of 0.4 ML. Edens et al. later reported similar STM images, but offered a different explanation.[102] Under appropriate imaging conditions, they could make every other row of spots on the surface disappear. They interpreted these images as indicating that the adlattice consisted of rows of SO_4^{2-} with alternating rows of coadsorbed hydronium cations in between which were only observed under some tunneling conditions. This yields a surface coverage of 0.2 ML sulfate which is more in line with independently determined coverage measurements.[103] More recent studies have indicated the presence of the same sulfate adlayer on Pt(111)[104] and Rh(111).[105]

V. Underpotential Deposition of Metals

One of the earliest uses of electrochemical SPM was to examine the underpotential deposition (upd) process. Upd is an electrochemical phenomena in which monolayers or submonolayers of a foreign metal adatom are deposited on a surface at potentials positive of the reversible or Nernst potential. Upd monolayers are formed by the deposition of low work function metals onto high work function substrates, and the electrochemical underpotential shift is directly related to the difference in work function between the substrate and adatom. Thus, monolayers of Cu can be formed on Au, but Au deposited onto Cu forms only bulk-structure islands. The upd monolayer can thus be thought of as originating from a relatively strong adatom-substrate bond formed using less energy than that required for subsequent adatom−adatom bonds formed during bulk deposition. A series of SPM images of a upd system might first show the bare metal substrate surface, followed by images of successively more and more close packed monolayers until the (1×1) monolayer and/or bulk (1×1) phase is reached.

One of the most intriguing aspects of upd is the anion dependence exhibited by several of the struc-

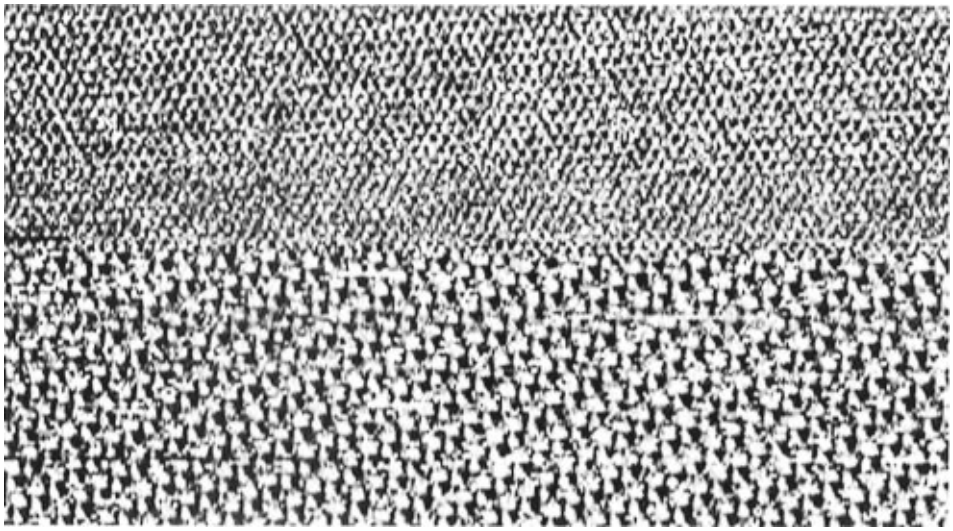

Figure 8. Image of the ordered adlayer on Au(111) in 1 M H_2SO_4. The upper half of the image shows the Au(111) substrate lattice observed at 0.68 V. The lower half of the image shows the overlayer observed after a potential step to 0.69 V. (Reprinted with permission from ref 101.)

tures observed which derives from coadsorption of the anion and the adatom. This behavior, first intuited from voltammetric and UHV emersion studies, has been the focus of much attention. The attraction of many groups to studying upd stems not only from the relative experimental simplicity of the process and the tendency of upd adlattice structures to exhibit considerable structural richness, but also from the importance of the upd process in deposition, catalysis, and fundamental studies of monolayers. The subject of upd has been reviewed,[106,107] although reviews incorporating the structural insight derived from the studies over the last decade are only now being written.

A. Upd on Gold Surfaces

1. Copper Upd

One of the first examples of atomic resolution on a metal surface in the electrochemical environment was afforded in STM images of Cu monolayers on Au(111) obtained in sulfuric acid solution.[10] Three different structures are seen before bulk Cu deposition as shown in Figure 9. The first, at the most positive potentials, is the bare Au(111) surface. The next structure formed, between 200 and 100 mV vs $Cu^{2+/0}$ is a $(\sqrt{3}\times\sqrt{3})$R30° adlattice. Finally, a (1 × 1) monolayer forms just prior to bulk deposition. The $(\sqrt{3}\times\sqrt{3})$R30° adlattice[22] and the (1×1) structure[108] both have subsequently been observed using the AFM and further structural details, including the observation of a phase boundary,[109] have been seen in other STM investigations. Studies of the kinetics of the transformation between the different phases and fits to models have also been performed.[110] An interesting result examined the dependence on the kinetics of the phase transition between the $(\sqrt{3}\times\sqrt{3})$-R30° phase and the (1×1) phase on Au(111) crystals with different degrees of miscut. More perfect crystals exhibited slower kinetics of phase change, a result which was interpreted as emphasizing the role of step edges in the kinetics.[111] The Cu upd system now provides a standard by which to determine the efficacy of tip coating and surface cleanliness and preparation techniques. It also has been used to quantitate defect surface areas in partial monolayers of thiols adsorbed on Au(111),[112] and the inhibitory effects of Cu on O_2 reduction on Au(111) have also been examined.[113]

Cu upd on Au(111) in sulfate is an example of a common behavior found in upd systems. One of the most interesting features exhibited in the upd process described above and found in several other adatom-substrate pairs is the existence of "open" adatom lattice structures. In metal-on-metal depositions performed in the ultrahigh vacuum environment, open structures are never observed except during formation of a surface alloy. Yet such structures are common in the electrochemical environment. In the case of Cu upd on Au(111) in the presence of sulfate, considerable effort, particularly that involving chronocoulometric measurements,[114] has shown that the $(\sqrt{3}\times\sqrt{3})$R30° lattice exhibited by this system forms due to coadsorption of sulfate with the upd Cu. However, the Cu coverage discerned in these chronocoulometric studies was not $^1/_3$ as suggested by the images but rather $^2/_3$. The coverage of the sulfate is $^1/_3$. Recent surface X-ray scattering measurements[115] show that the sulfate forms a $(\sqrt{3}\times\sqrt{3})$R30°-1SO_4 lattice while the Cu atoms are arranged in a honeycomb lattice exhibiting a $^2/_3$ surface coverage. Theoretical work by Blum and Huckaby strongly emphasized that this honeycomb structure was the only one consistent with the voltammetry.[116] This example shows that the SPM techniques are most powerful when utilized in conjunction with other methods providing more quantitative information about the number and type of species present on the electrode surface.

The sensitivity of the upd adlattice structure to anions in solution which become coadsorbed has prompted effort examining the sensitivity of the Cu system to anions other than sulfate. The initial AFM work showed that different solutions did indeed give rise to different structures on the electrode surface, a result that was anticipated from earlier emersion and electrochemical work. *In situ* STM and AFM work has examined the role of chloride in the upd

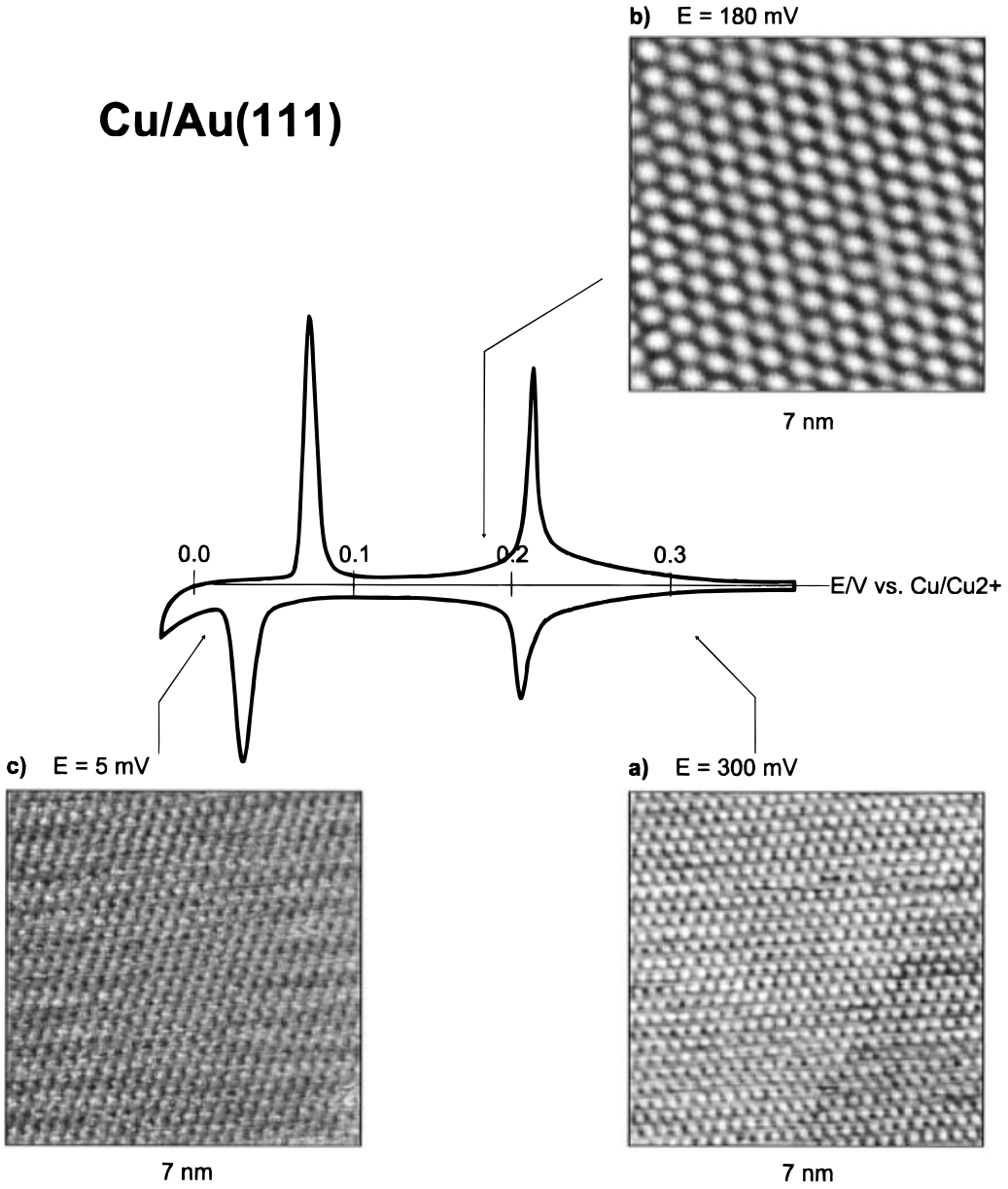

Figure 9. Cyclic voltammogram (5 mV/s) of Au(111) in 0.05 M H_2SO_4 + 1 mM $CuSO_4$ and STM images for three different potentials. (a) $E = +0.30$ V vs Cu/Cu^{2+}. The surface atoms of the bare Au(111) are visible. (b) $E = +0.18$ V vs Cu/Cd^{2+}. Ordered adlayer with $(\sqrt{3}\times\sqrt{3})R30°$ structure, ascribed to coadsorbed sulfate. (c) $E = +0.005$ V vs Cu/Cu^{2+}. Full Cu monolayer in registry with Au(111). (Reprinted with permission from ref 10. Copyright 1990 American Physical Society.)

monolayer, with the observation that both (2×2) and incommensurate (5×5) structures formed in the presence of this anion,[117] depending on the Cl^- concentration.[118] The (5×5) structure has also been observed in the presence of crystal violet, a tricyclic organic additive, although this is thought to be a consequence of Cl^- present in the additive. Rationalization of this structure, and the structure of other upd adlattices formed in the presence of anions continues to be a major focus of inquiry.

On the other low Miller index faces of Au, Cu does not exhibit the pronounced dependence on anion found on the (111) face. STM work examining Cu upd on Au(100)[119] and Au(110)[120] in the presence of sulfate revealed only a (1×1) lattice structure which was interpreted as resulting from a pseudomorphic Cu adlattice. In solutions containing Cl^-, however, a one-dimensionally incommensurate (n×2) structure was observed to form on Au(100), while a (2×1) overlayer—thought to be roughly equivalent to a CuCl(111) bilayer—was found on Au(110). AFM work on Au(100) confirmed the (1×1) lattice structure.[121] The reduced sensitivity of the (110) and (100) faces to sulfate coadsorption clearly relates to the reduced strength of association of sulfate with the electrode surface, a subject of considerable interest in electrochemical surface science.

2. Silver Upd

The rich chemistry observed for Cu has prompted considerable effort examining other upd systems on Au surfaces. One of the first of these was Ag upd. The first studies used AFM to show that several different structures of Ag upd were obtained in solutions containing different anions. In sulfate, the AFM work showed a (3×3) structure, in nitrate and carbonate a (4×4) structure, in perchlorate an incommensurate structure, and in acetate a (1×1) struc-

ture.[122] These results were interpreted as demonstrating that the size of the anion affected the structure of the upd adlattice, with larger anions leading to more open structures. The structure of the Ag adlattice on Au(111) in sulfate containing electrolyte has been questioned, with two STM studies indicating that a $(\sqrt{3}\times\sqrt{3})$R30° adlattice is formed instead.[123,124] These studies also examined the low potential region and followed the condensation to a (1×1) overlayer. *Ex situ* Auger electron spectroscopy measurements confirmed that sulfate was coadsorbed with the Ag and LEED studies confirmed the (3×3) structure for this system.[125] A study on the height of the upd adlayer demonstrated that the Ag monolayer grew by a step-growth mechanism and that the history of the substrate played an important role in the shape of the voltammetry.[126] The exact structure of the monolayer and its phase transitions remain to be elucidated.

On Au(100), AFM studies reveal that a (1×1) monolayer of Ag is formed from the condensation of a c$(\sqrt{2}\times5\sqrt{2})$R45° lattice formed at positive potentials.[127] This structure is found even in perchlorate-containing electrolyte which suggests that simple incorporation of anion is not entirely responsible for the open structure formed. The (1×1) monolayer has also been observed in STM work, although these authors could not exclude the (1×1) structure as deriving from a result of alloying.[128,129]

3. Lead Upd

Upd of Pb onto Au surfaces was an important early example of work studying upd. Pb voltammetry on Au(*ijk*) surfaces was extensively investigated by Hamelin,[130] who showed how voltammetric features arising from one face smoothly transformed into those from another. The Pb upd system is also important because—like the Bi adlayer discussed in the next section—it participates in H_2O_2 electroreduction, but only at specific potentials corresponding to particular structures on the surface.[131] The first STM studies of Pb upd on Au(111)[132,133,134] showed that distinct changes occurred on the surface following an excursion of the potential into the upd region. These first studies indicated that the surface developed a monatomic high layer—associated with the Pb adatoms in a (1×1) structure—and that following removal of the adlayer a series of pits and depressions remained which were associated with consequences of production of a surface alloy. Atomic resolution studies of the surface using STM showed that an incommensurate (1×1) layer was indeed formed.[135] Moreover, this layer formed a moiré pattern with the surface where the Pb adlayer went in and out of phase with the underlying Au(111) texture. Features in the voltammetry occurring positive of the full monolayer formation peak were associated with the formation of islands on the surface, the (1×1) structure of which was ascertained from AFM studies.[136] The AFM work also associated the presence of Pb islands with the maximum in peroxide reduction catalytic activity arising from the modified surface.

4. Bismuth Upd

Bi is another element whose upd structure on Au(111) has been examined using AFM and STM. Monolayers of Bi formed through upd on Au(111) act as a catalyst for the two-electron electroreduction of H_2O_2 to H_2O in acid solutions. However, this catalytic activity occurs only in a narrow potential region.[137] There are two lattices observed in the upd region. The first of these corresponds to a (2×2)-Bi adlattice shown in Figure 10b.[138] The second structure seen prior to bulk deposition of Bi is shown in Figure 10c. The lattice has now changed to a "uniaxially commensurate" $(p\times\sqrt{3})$ structure which exhibits a $\sqrt{3}$ spacing in one direction (U1 in Figure 10 (left)) but is incommensurate in the U2 direction. These structures have been confirmed by the completely independent surface X-ray scattering (SXS) technique.[139] Interestingly, peroxide electroreduction occurs only in the potential region where the (2×2)-Bi adlattice is present. As is the case with the Pb adlayer, electroreduction of peroxide occurs only when both the Au adlattice and the upd metal are exposed; neither the bare surface nor the full monolayer exhibit catalytic activity.

5. Thallium Upd

Yet another upd metal examined has been Tl, which forms an interesting series of structures on Au(111) in alkaline solution.[140] STM work performed in conjunction with SXS measurements showed that a series of structures formed on the surface, starting at positive potential with a disordered, unimageable adlayer associated with Tl oxidation and then, in rapid succession a hexagonal phase, an incommensurate hexagonally aligned phase ($\theta = 0.56$) incorporating OH^- anion, and a close-packed incommensurate Tl adlayer without the OH which is misaligned from the Au substrate by 6°.

6. Cadmium Upd

Cd upd has been examined on both Cu(111) and Au(111) electrodes. On Cu(111), the Cd forms a (4×4) structure prior to bulk deposition. However, on Au(111) in the upd potential range a series of *linear* structures are observed[141] as shown in Figure 11, the origin of which must derive from coadsorption of both the sulfate anion and the Cd adatom. The origin of the linear structure itself is not yet clear, although this may derive from the very negative potentials at which the upd process occurs.

7. Mercury Upd

Two studies of Hg upd utilizing AFM and STM are in the literature. The first utilized AFM to demonstrate that Hg upd structures also depended on the choice of anion, with different structures observed for sulfate and acetate. The acetate structure was interpreted in terms of the formation of an Hg–acetate complex on the Au(111) surface.[142] More recently, the Itaya group obtained images of the Hg adlayer in sulfate with greater detail, and showed that this adlayer evolved from the $(\sqrt{3}\times\sqrt{7})$ sulfate structure found on the bare Au(111) surface.[143] While the AFM was not able to resolve structures at

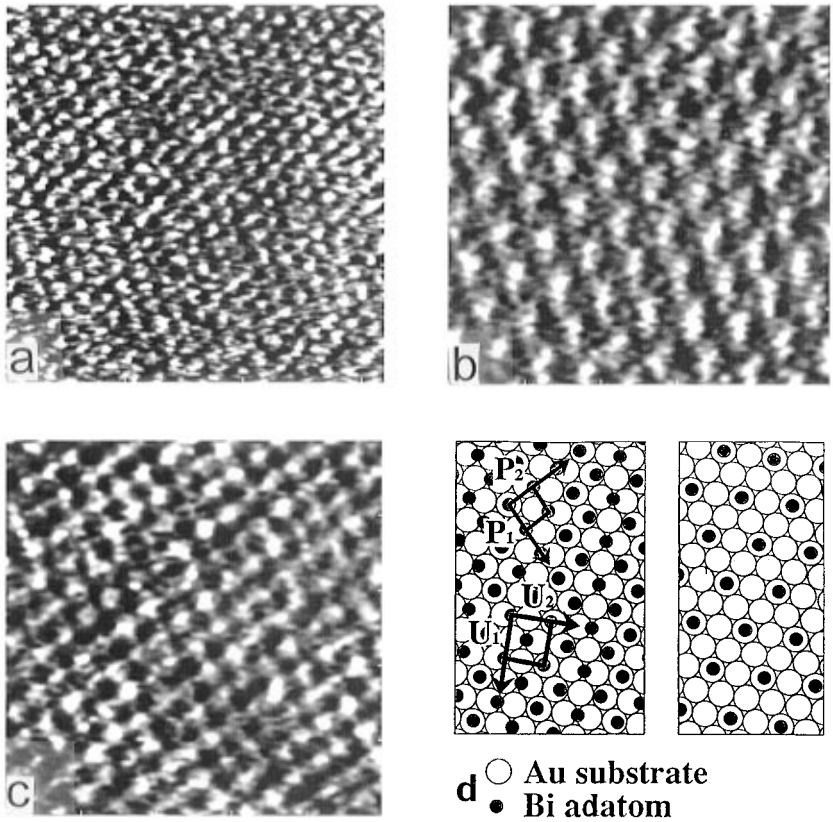

Figure 10. AFM images (5 × 5 nm) of Bi upd on Au(111) in 0.1 M $HClO_4$. (a) Au(111) surface found positive of Bi upd peaks. (b) (2×2)-Bi adlattice found at 200 mV vs Bi/Bi^{3+}. (c) Uniaxially commensurate rectangular Bi adlattice found at 100 mV. (d) Schematic of Bi structures: left, rectangular lattice where P and U are primitive and nonprimitive unit cell vectors, respectively; right, (2×2)-Bi adlattice. (Reprinted with permission from ref 138. Copyright 1992 American Chemical Society.)

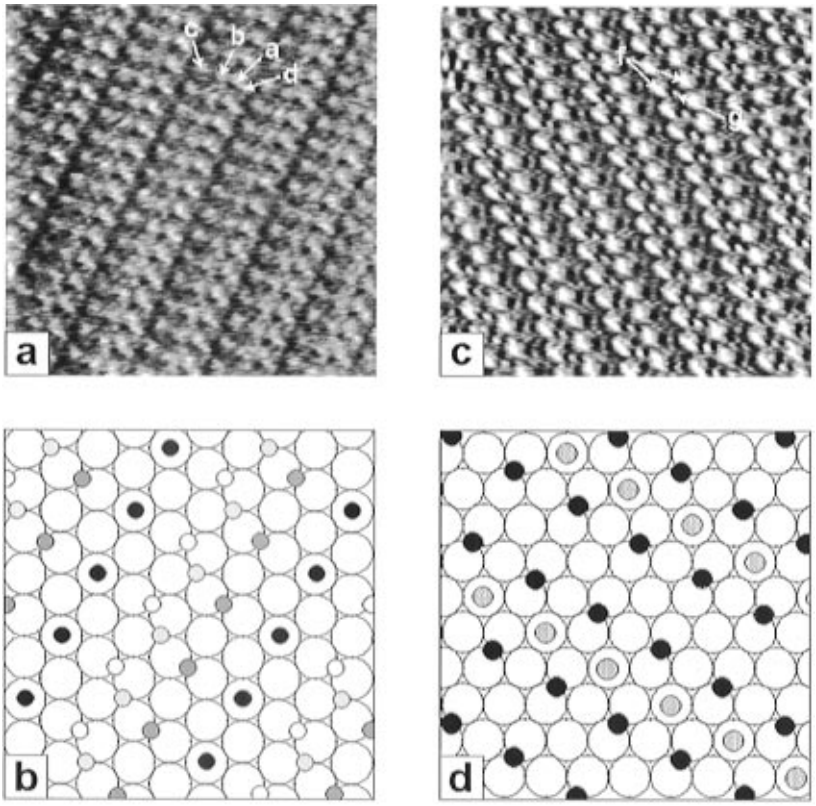

Figure 11. (a) A 7.5 × 7.5 nm STM image of overlayer obtained at 250 mV vs Cd/Cd^{2+} in 0.1 mM Cd^{2+} + 0.1 M H_2SO_4. (b) Proposed structure for overlayer seen in a. (c) A 7.5 × 7.5 nm STM image of overlayer obtained at 225 mV vs Cd/Cd^{2+}. (d) Proposed structure for overlayer seen in c. (Reprinted with permission from ref 141. Copyright 1996 American Chemical Society.)

the more positive potentials and the STM was successful, the STM failed to resolve structures closer to bulk deposition, in part because of Hg reactivity at the Pt tip.

B. Upd on Other Metal Surfaces

The success in imaging upd adlattice structures on Au surfaces has prompted considerable work examining upd on other metals. This work has in part been directed to comparing the upd structures found on these other surfaces with that seen on Au in order to discern the influence of the underlying adlattice and in part to understanding specific reactivity on these other surfaces. Work on Pt surfaces, for example, focuses on the influence of the adlattice on catalytic activity.

1. Silver Surfaces

Much work has attended studies of Pb upd on Ag surfaces. STM work on Ag(111)[144−146] demonstrated that the full monolayer in this system also gave rise to a (1×1) monolayer which, like its counterpart on Au(111) also formed a moiré pattern. Detailed analysis on this pattern allowed the authors to discern the degree of rotation (ca. 2.5°) between the overlayer and the substrate which was consistent with the observed periodicity of the moiré pattern. With long time cathodic polarization of Pb on this surface, evidence for formation of a surface alloy—as in the Au case—has also been obtained by examining the behavior of the upd deposit in the neighborhood of step edges showing the formation of a different phase from the (1×1) structure seen at short times.[147] Upd deposits of Tl also exhibit similar behavior. On Ag(100), Pb upd gives rise to a c(2×2) structure which—based on comparison to coulometric results—is thought to form as a bilayer. The bilayer ultimately coalesces into a (1×1) adlattice prior to bulk deposition.[148]

A number of studies have examined formation of mixed-upd monolayers on both Au and Ag surfaces. In this work, upd of a more noble metal is initiated on the surface in a solution containing two metals and then followed by deposition of the second atop the first.[149,150] A related scheme has been employed by Stickney and co-workers to create adlattices of CdTe and CdSe on Au surfaces.[151]

2. Platinum Surfaces

Work on Pt surfaces has paralleled that performed on Au. Cu upd on Pt(111) in sulfuric acid electrolyte reveals the same ($\sqrt{3}\times\sqrt{3}$)R30° structure found on Au(111),[152] with approximately the same charge representing $^2/_3$ monolayer coverage. The observed structure is now thought to derive from the same images of sulfate that control the STM and AFM images obtained from the Au surface.[153] As in the Au situation, the Cu-modified surface is found to be much less active for O_2 reduction than the unmodified surface, presumably because the Cu adatom blocks sites to which the peroxide moiety binds.[154] On Pt(110), only a diffuse (1×1) structure is found,[155] again in parallel with results seen for Au. Work examining Cu upd on Pt(111) in the presence of the organic additives thiourea and polyethylene glycol while not achieving atomic resolution was entirely consistent with the formation of the diffuse adlayer observed previously.[156]

Studies of the influence of halides on upd structures on Pt have focused on upd of Ag on iodine-covered Pt(111) surfaces where a (3×3) structure is found to form initially followed by condensation to a ($\sqrt{3}\times\sqrt{3}$)R30° adlattice.[157] Correlation of the STM images with insight obtained previously from *ex situ* LEED and Auger measurements indicates that the observed structure actually results from an I adlayer atop the Ag monolayer. Examination of upd structures formed by coadsorption of Cl, Br, and I with Cu on Pt(111) and Pt(100) revealed a wealth of structures including a (4×4) structure for Cu on Pt(111) in Cl^- containing solution and a ($\sqrt{3}\times\sqrt{3}$)-R30° for Cu on Pt(111) in Br^-.[158] These studies point out the inability of the SPM work alone to determine the composition of overlayer structures in systems with coadsorbed constituents that lack clear spatial distinction.

Another upd system studied is Pb on Pt(111) examined using both SXS and STM.[159] These techniques revealed a (3×$\sqrt{3}$)- 4Pb structure corresponding to $\theta = {}^2/_3$. However the STM also revealed a coexisting (2$\sqrt{3}$×2$\sqrt{3}$)R30°-7Pb structure near step edges which was not detected by the SXS method. No ordered structures for Pb have been found on Pt(100) and Pt(110). The commensurate, open, structures seen with Pb on Pt were contrasted with the incommensurate hcp layers found with this adatom on Au(111) and Ag(111) and may be an indication of the stronger adatom-substrate bond present on Pt. Thallium upd on Pt(111) has also been studied.[160]

3. Copper Surfaces

The only report of upd on Cu surfaces examines the structure of Cd on Cu(111). Here a (4×4) adlattice was found to form, which ultimately coalesced into a (1×1) structure prior to bulk deposition.[161] Studies on this and other surfaces which form a facile oxide are inhibited by the necessity of removing the oxide material prior to upd, because the oxide covered surface typically exhibits a much lower work function than the bare metal.

VI. Bulk Deposition of Metals

Studies of the structure and reactivity of monolayers, discussed in the last section, inevitably proceed to studying the properties of bulk deposits. Bulk deposition of materials such as Cu and Ni is a technologically highly relevant process with work directed toward characterizing and controlling the texture and development of the deposit. A detailed understanding of the mechanism of growth of bulk electrochemical deposits remains to be elucidated, in part because of the complexity of the process and in part because the tools necessary for understanding these are only now being developed. Work in the area of bulk deposition using SPM is divided into research addressing the initial phases of bulk deposition, the subsequent growth of the deposit, and the influence of specific additives on texture and growth.

Considerable effort has attended especially the deposition of Cu because this material deposits at a potential positive of H_2 evolution (and hence is experimentally tractable) and because of the understanding developed concerning Cu monolayer formation on Au. However, work on Ag, Ni, Au, Pt, Tl, and Pd deposits has also been undertaken. Common substrates include Au and HOPG, although Pt and various semiconductors materials are developing into popular surfaces as well.

A. Copper

The first work addressing Cu deposition on polycrystalline Pt occurred relatively early in the development of electrochemical STM and showed that deposition of Cu led to a nonuniform deposit which apparently smoothed following removal of the applied potential.[162] More sophisticated efforts address the details of the deposition process. On polycrystalline Pt, Uosaki and Kita[163] showed that deposition of Cu led to gross changes in the substrate morphology. On HOPG, Stimming[164] showed that deposition of Cu could be followed and found that Cu was deposited initially in small clumps on the surface. One particularly disturbing note was that the STM tip appears to affect the growing deposit, and deposition was inhibited in the area under the STM.[165] In this instance, the tip appears to potentiostatically shield the surface.[166] This means that STM studies of Cu deposition must reflect the overriding presence of the tip.

High-resolution work by Kolb and co-workers showed that in the absence of additives, deposition of Cu occurs first at step edges, dislocations, and defects in the Au(111) substrate surface, followed by deposition at longer times on terraces.[167,168] Dislocations could also be induced by deliberately "crashing" the tip gently into the Au surface and transferring Cu deposited on the tip to the surface.[169] This leads to a series of very small Cu clusters on the surface, the growth of which was monitored by STM. The clusters grow in a layer-by-layer manner, much more rapidly parallel to than normal to the surface.[170] The importance of dislocation sites was nicely emphasized in subsequent work where preferential initial deposition around the edges of the islands formed on Au(100) following the lifting of the surface reconstruction was shown.[171]

In the presence of an organic additive, the deposition mechanism changes considerably. Addition of crystal violet yields a growth morphology in which deposits develop by spreading essentially parallel to the surface, yielding a Cu film much smoother than those formed in the absence of additive.[172] As can be seen in Figure 12, the presence of the additive drastically alters the morphology of the growing Cu deposit. The effect of the additive is not to inhibit nucleation at defects, but rather to affect the subsequent growth of the deposit.[173,174] Benzotriazole yields similar behavior on both Au(111)[173] and Pt(100) surfaces.[175] However, the behavior of the growing deposit was somewhat more complicated, and depended on the concentration of the organic additive and the overpotential used in deposition. At low overpotentials, only growth from individual

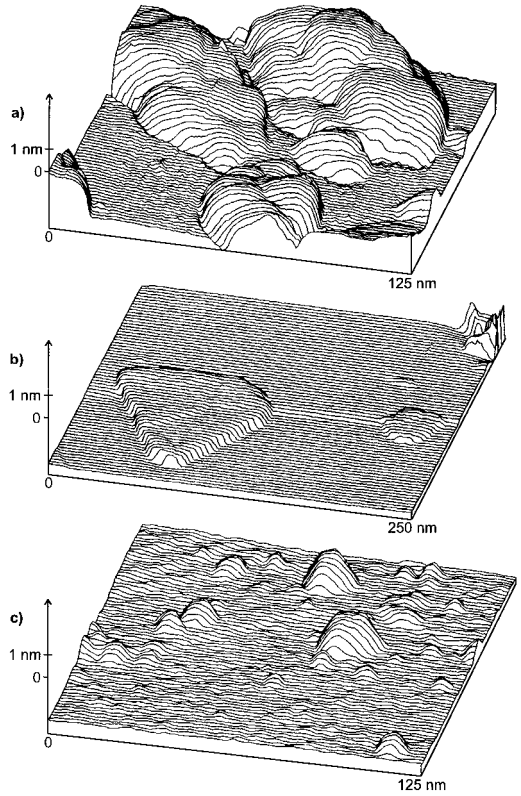

Figure 12. Comparison of Cu deposits on Au(111) formed (a) in the absence of organic additives, (b) in the presence of crystal violet, and (c) in the presence of thiourea. (a) $E = -0.15$ V; 5 mM H_2SO_4 + 0.05 mM $CuSO_4$. (b) $E = -0.13$ V; 0.05 M H_2SO_4+ 1 mM $CuSO_4$ + 0.1 mM crystal violet. (c) $E = -0.10$ V; 5 mM H_2SO_4 + 0.05 mM $CuSO_4$ + 0.1 mM thiourea. All potentials vs Cu/Cu^{2+}. (Reprinted with permission from ref 176. Copyright 1995 Kluwer Academic.)

nuclei was observed, while at higher values, uniform nucleation and overlap were seen. The additive thiourea gives rise to a somewhat different growth pattern. Here, nucleation occurs on the terraces of the Au(111) substrate, at the rims of underpotentially deposited Cu islands.[176] In the presence of HCl on HOPG, Josefowicz et al. using AFM showed that deposition yielded triangular-shaped clusters, which were thought to originate from a CuCl species.[177] The deposition structure transforming properties of chloride as an additive were confirmed in a more recent study on HOPG,[178] although this work was performed at neutral pH values which means that the effect of bulk CuO formation cannot be ruled out. Deposition carried out in sulfuric acid alone led to loosely held Cu deposits on the HOPG surface.

More recent work has examined Cu deposition onto substrates other than Au, Pt, or HOPG and under other deposition conditions. Andersen et al.[179,180] showed that Cu deposition at low overpotentials on Au could be understood as a balance of deposition and dissolution and that at long times, the Cu deposit apparently changed into a recrystallized phase of a Cu−Au alloy. Schmidt showed that the presence of solution flow through an AFM cell and over the substrate could strongly affect the texture of the growing Cu deposit, with the texture ranging from rough nucleation on Pt in stagnant solution to a much smoother deposit obtained with higher fluid flow rates of 0.094 cm^3/s.[181] The influence of the pulse-

plating methodology was examined using STM and the smooth deposits obtained following a 20 ms cathodic pulse were interpreted as arising from a leveling effect due to the initial growth of a Cu powder.[182] An interesting method developed to test the effect of additives on the initiation of deposition involved depositing Cu atop a thiol monolayer.[183] The presence of the thiol results in the formation of hemispherical nuclei. Another study examining deposition atop thiol-modified surfaces concluded that defects in the monolayer controlled the nucleation and deposition behavior.[184]

On surfaces other than Au, Pt, or HOPG, Cu exhibits a different deposition behavior. On *p*-GaAs(100) in HCl, AFM measurements showed that Cu deposited on relative smooth parts of the surface form randomly distributed clusters followed by three-dimensional growth of the clusters. However, on areas of the surface with defects, the Cu deposit tended to follow the morphology of the defect. A very interesting study examined the deposition of Cu onto Ag(111).[185] Unlike the case with bare Au(111), Cu deposited at low overpotentials nucleated on the terraces of the Ag substrate and followed a two-dimensional growth mode. The overlayer grows pseudomorphically and covers the whole surface before the second Cu layer starts to grow on top. This behavior was explained by invoking the specific adsorption of sulfate on the Ag substrate steps and defects, sealing these imperfections much in the same way that thiourea works on Au substrate. One deposit on polypyrrole has also been examined, with deposit characterized by instantaneous nucleation followed by three-dimensional growth.[186,187]

Finally, several groups have used more advanced analytical tools to examine the growing Cu electrodeposits. Scaling analysis of growing Cu deposits has provided some insight into the mechanism of their growth.[188,189]

B. Silver

Silver is another important metal whose deposition behavior has been studied using SPM. Surface diffusion of Ag is considerably faster than that of Cu, and deposit morphologies clearly reflect this difference. Work has examined Ag deposition onto HOPG, Au, and other metals.

Some of the earliest work examining deposition was performed to study Ag deposition onto HOPG. The first effort by Sonnenfeld and Schardt[190] showed that Ag deposition could indeed be visualized using *in situ* STM, although these authors were not able to image the initial stages of deposition. As with work examining Cu deposition, these early efforts showed that the tip could affect the deposition morphology.[191] The morphology of the deposit could also be altered by changing the deposition rate,[192] and several authors noted that deposition commenced at step edges and other defects in the HOPG basal plane.[193] The initial deposition kinetics were described by a model involving progressive nucleation on active sites and diffusion-controlled three-dimensional growth.[194] Penner and co-workers showed that deposition of small clusters of Ag onto the basal plane of HOPG could be affected using the STM by applying voltage pulses between the tip and the sample in a solution containing Ag. This leads to the controlled formation of Ag nuclei at the defect formed by the voltage pulse,[195] with the Ag originating as a upd deposit on the Pt tip.[196] Subsequent work from the same group showed that small Ag crystallites formed on the HOPG basal plane as well; these were imageable only with noncontact AFM as they were easily swept away by either contact AFM or STM.[197] Such studies emphasize the importance of utilizing complementary techniques to study complex phenomena.

Deposition of Ag onto other materials has also been the focus of considerable effort. On a Ag single crystal grown electrolytically from a $AgNO_3$ solution, an early effort observed the presence of what apparently were "active" and "inactive" regions on the surface, the interpretation of which focused on inhomogeneous adsorption of impurities.[198,199] On Au(111) initial work examining deposition observed homogeneous growth of small Ag islands.[200] *In situ* STM confirmed that the initial growth of Ag on Au surfaces was as an epitaxial film following formation of the full upd monolayer.[201−203] Alloy formation was not found to be significant in the process. A layer-by-layer growth mode has also been observed for this process by some workers[204,205] although others have seen a Stranski−Kranztanov mechanism operative in perchloric acid electrolyte.[206] More recent work using the AFM has confirmed the nearly ideal Frank−van der Merwe growth mode, which is ascribed as a result of the extremely rapid surface diffusion of Ag on the growing Ag crystal surface.[207] A very interesting observation from the Kolb group shows that while the first eight layers of the growing Ag surface are indeed epitaxial with the underlying Au(100) surface, the ninth layer is rotated or reconstructed and forms the beginning of the true Ag(111) electrodeposit.[208]

C. Other Metals

Aside from the deposition of Cu and Ag, work has examined deposition of a variety of other materials on HOPG. The technological importance of both Ni[209] and NiP[210] has prompted *in situ* studies examining nickel deposits formed on HOPG. In both cases the deposit grows from small islands suggesting nucleation and growth of small grains. Pd deposition onto HOPG showed similar behavior,[211] although later work by the same group indicated that the current surge occurring when they enabled their potentiostat *in situ* was responsible for some of the observed nucleation behavior.[212] Biclusters electrodeposited onto HOPG behave similarly in that they nucleate at defects and coalesce during the growth phase.[213] Finally, Pt hydrosols have also been deposited onto HOPG electrochemically leading to high Pt surface coverage.[214]

Möller et al. have reported several interesting behaviors of Ni when deposited onto reconstructed Au(111) surfaces. First, they showed[215] that Ni nucleation proceeds in three distinct, potential dependent steps: (a) place exchange of Ni with Au atoms at the elbows of the reconstructed Au surface at low overpotentials, (b) nucleation of Ni islands on top of the substitutional Ni adatoms at medium

overpotentials, and (c) nucleation at the step edges of the Au substrate. This control of deposit texture with potential makes possible the fabrication of fine features on the electrode surface. Second, they showed[216] that Ni could grow in a highly anisotropic manner on Au(111) forming in part a needlelike structure oriented along the (110) direction; this anisotropy was thought to be related to the very negative potential of Ni deposition which could lead to H adsorption atop the Ni atoms and a corresponding weakening of the Ni−Au bond.

More involved behavior was also observed in studies of Pd and Hg onto Au surfaces. Formation of an Hg/Au amalgam was demonstrated using AFM following deposition of Hg onto Au(111).[217,218] The images showed that small alloy protrusions form initially at the Au grain boundaries. The growth of the protrusions is always accompanied by the dissolution of Au at grain boundaries, leaving many pits visible on the amalgamated surface. Work examining Pd deposition on Au(111) by using *in situ* STM showed that while the first bulk layer of Pd grew in the form of two-dimensional islands, the second layer grew partly in two dimensions and partly in three.[219] Finally, it should be noted a large number of studies have examined the morphology of several metals *ex situ* as well.

VII. Corrosion

Considerable effort has also attended studies of the dissolving or corroding solid/liquid interface using probe microscopy. Just as in the case of deposition, where research attempts to examine the initial stages and time-course of the process, so too in corrosion are attempts directed at examining the initiating steps and the shape evolution of the corroding material. Initiation of corrosion is typically not as precise as the initiation of deposition, because the initial sites of corrosion or dissolution are often widely separated and may be outside of the view of the probe microscope. In addition, the rate of corrosion can be difficult to control on many materials. Materials with a passivation layer, such as stainless steel or aluminum may take large overpotentials to initiate breakdown of the passivation layer. Once this layer is breached, the actual dissolution of material takes place quickly, and without many opportunities to control its rate. Probe microscope studies of corrosion and dissolution have focused on important problems with Cu, steel, Al, and other materials, especially semiconductors.

A. Copper

The first effort examining Cu dissolution using probe microscopy was by Moffat, Fan, and Bard, who examined the dealloying of Cu_3Au.[220] By correlating the electrochemical and coulometric responses of an electrode made of this material, these authors showed that clustering of Au atoms occurred near sites of Cu dissolution at low overpotentials, while at high overpotentials global surface roughening was observed. The critical overpotential which defines the transition between the two regimes was found to be a function of solution composition. Similar behavior was observed by Pickering and co-workers[221] who showed that plateau development and smoothing of the plateaus during Cu dissolution from a Cu−Au alloy was inhibited by addition of K_2CrO_4 to the solution. This behavior also examined the changes in surface roughness.

Breuer, Stimming, and Vogel monitored the dissolution of Cu clusters deposited on polycrystalline Au electrodes using *in situ* STM.[222] These authors observed that the presence of the STM tip slowed the degree of dissolution—in the same way the tip had inhibited the deposition of Cu onto this surface.

Another study examining the dissolution of Cu deposited onto HOPG found that dissolution was dependent on the overpotential used.[223] At low overpotentials in Cl^--containing solution, AFM images showed structures that were interpreted as being due to Cu corrosion alone, while at higher overpotentials, triangular structures associated with CuCl formation were observed. However, definitive assignment of features could not be made.

Higher resolution work by Suggs and Bard[224] in Cl^- electrolyte showed that on Cu(111), Cl^- forms a $(6\sqrt{3}\times6\sqrt{3})R30°$ overlayer. Anodic dissolution of Cu from this surface appeared to preferentially begin at step edges with the retreating edges running along steps in the {211} direction. On the Cu(100) surface, these same authors[225] found that Cl^- forms a $(\sqrt{2}\times\sqrt{2})R45°$ adlattice. Here the preferred reaction sites for dissolution were step edges with edges always retreating along the Cu(100) {100} direction. This direction features a very similar open structure to the {211} direction found on the (111) surface.

Vogt and co-workers examined the Cu(100) surface in even higher detail.[226] They found that the surface immersed in Cl^- undergoes a transition from a (1×1) to a $(\sqrt{2}\times\sqrt{2})R45°$ structure as the potential is swept to more anodic values from −0.4 V vs Ag/AgCl. This change in surface structure is not accompanied by any change in surface Cl^- coverage, as determined by electrochemical measurements, leading the authors to conclude that the (1×1) phase represents a disordered phase of Cl^- on the Cu surface.

Larger-scale observations of Cu corrosion behavior by Cruickshank et al.[227] showed that anodic polarization of polycrystalline Cu electrodes leads to dissolution of the 40−60 nm thick amorphous overlayer formed during polishing. Further dissolution proceeded along grain boundaries, and was substantially inhibited by the addition of benzotriazole to the solution.

B. Steel

While Cu itself is a very complex surface, this complexity pales when compared to that found for stainless steel. In an early effort, Fan and Bard[228] showed that corrosion of stainless steel samples appeared to be initiated at defects or edges and that extended corrosion leads to a moundlike structure. Similar conclusions were presented by Miyasaka and Ogawa.[229]

The structure of the passive films formed on Fe−Cr alloys—the chief components of stainless steels—has been examined by a number of groups. Ryan et al.[230,231] used STM to show that the crystallinity of

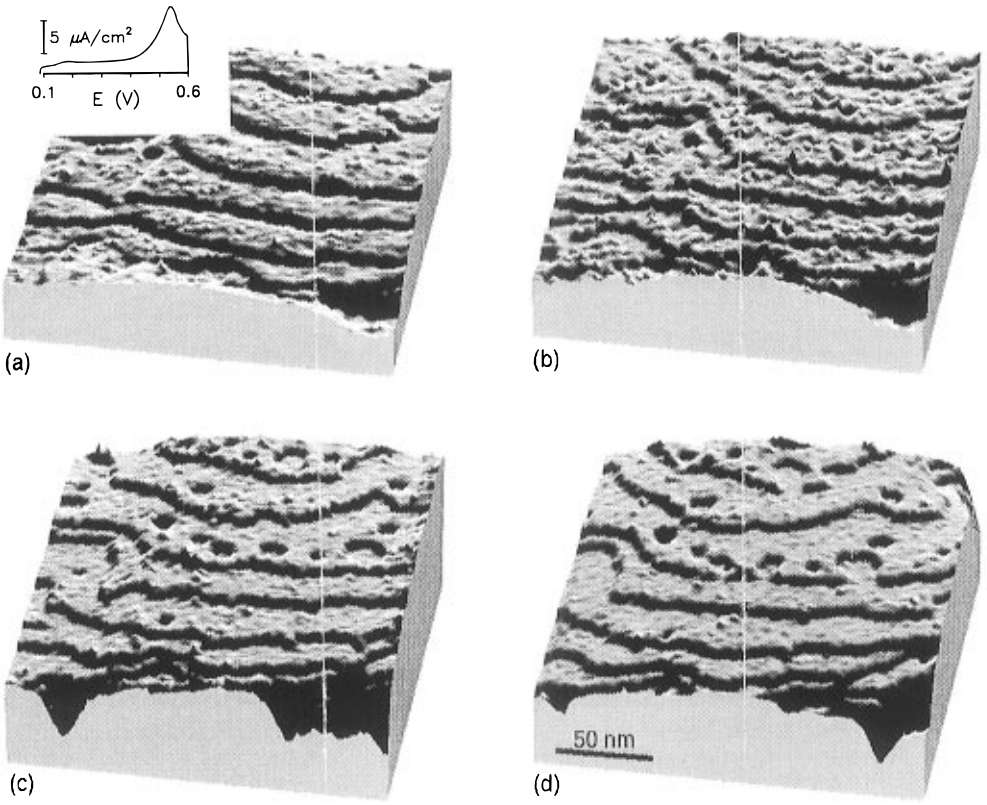

Figure 13. Time sequence of *in situ* STM images of the corrosion of an $Ag_{0.07}Au_{0.093}$ alloy in 0.1 M $HClO_4$. (a) Immediately, (b) 10, (c) 51, and (d) 86 min after scanning the potential to 0.6 V. (Reprinted with permission from ref 239. Copyright 1991 American Association for the Advancement of Science.)

the passive layer formed in sulfuric acid is a function of the Cr content of the alloy. This work revealed that the passive layer on the surface was largely composed of Cr_2O_3. Work by the Bockris group examined the films formed on pure Fe surfaces, although without high resolution.[232] Ryan and co-workers[233] were able to resolve the structure of the passive film formed on Fe in borate and showed it was consistent with a proposed γ-Fe_2O_3/Fe_3O_4 structure rather than forming an amorphous or disordered material. More recently, Walls et al.[234] examined the evolution of the surface morphology of Fe−Cr alloys during oxidation reduction cycles. They showed that the inclusions present in the industrial Fe−17%Cr material were the initial sites of corrosion leading to a pitted surface while purer materials are free from this type of attack. The specific behavior of inclusions remains an important focus of corrosion research.

C. Aluminum

Important work has also attended Al surfaces. Bhardwaj and co-workers[235] examined the effect of oxidation and reduction processes on the polycrystalline Al electrode surface in 0.01 M NaOH. This work showed that the initial stages of what was associated with oxide formation initiated in the form of patches or clusters. The differences between the corrosion of Al and Al−Ta materials in NaCl solution were noted in another study.[236] The apparent roughening observed *in situ* for the Al−Ta alloy was about 40% less than that seen for pure Al.

Chen and Guay[237] showed that imaging an Al surface with an AFM tip initiated selective dissolution of the Al material, producing a cavity with sharp boundaries. The authors provided evidence that the removal mechanism was a direct consequence of the energy dissipation from frictional forces caused by scanning the AFM tip over the surface. Later work[238] showed that the enhanced dissolution probably arose from an increase in the local reaction rate of adsorbed Cl^- and Al ions, leading to formation of a soluble complex and to the thinning of the Al layer.

D. Gold

One of the classic STM papers examining corrosion was the dealloying study of Ag−Au alloys performed *in situ* by Chidsey, Sieradski, and co-workers.[239] These authors examined with high resolution the morphological changes which occurred to the surface of this material accompanying the selective dissolution of Ag from the alloy in acid solution. The selective dissolution of Ag led to roughening of the surface by dissolution of Ag atoms from terrace sites as shown in Figure 13. The figure shows that as the surface corrodes, smoothening of the surface occurs by vacancy migration through clusters and the subsequent annihilation of clusters at terrace ledges.

Crooks and co-workers have studied the corrosion of bare and alkanethiolate-modified Au(111) surfaces under a variety of electrochemical conditions. In F^--containing solutions these authors observe[240] that the STM tip can induce surface-atom diffusion and at very negative surface potentials the tip enhances the selective removal of Au atoms from surface defects. However, in CN^--containing solution, the effect of the tip is much more dramatic, with the area under the tip being selectively etched. Passivation

of the surface with a monolayer of alkanethiolates was found to inhibit Au dissolution.

E. Other Materials

Itaya and co-workers[241] examined the anodic dissolution of S-modified Ni(100) surfaces and showed that the c(2×2)-S adlayer passivated the Ni surface toward oxide formation. Dissolution of the modified surface occurred only at step edges, resulting in the formation of an atomically flat terrace-step structure. Dissolution occurred along the [010] direction faster than along [001]; a result which relates to the relative energy required to remove Ni atoms on the corresponding edges.

Dissolution of iodine-modified Pd surfaces has also been examined.[242] In sulfuric acid containing no I^-, dissolution of the surface is not observed at anodic potentials. In the presence of I^-, the rate of dissolution was found to be sensitive to the orientation of the Pd crystal surface, increasing in the order Pd(100) < Pd(111) < Pd(110). Dissolution was found to occur preferentially at step edges, with a rate also sensitive to step alignment.

Murray and co-workers[243,244] examined the electrochemical oxidation of highly oriented pyrolytic graphite in several different electrolytes and showed that oxidation of the graphite surface produced, raised, hollow, bubblelike features, giving the appearance of shallow blisters. The blisters were established to be hollow, with a top surface of intact HOPG lattice and an inner one of graphitic oxide. Blister formation was observed to occur only in the presence of anions which suggest that they form from electrolyte anion intercalation followed by subsurface gas evolution. Wang et al. have characterized glassy carbon electrodes *in situ* by STM after electrochemical pretreatments.[245] They found that both AC and DC pretreatment resulted in surface roughening.

VIII. Semiconductors

Much is known about the growth and surface morphologies of semiconductors from ultrahigh vacuum experiments. Electrochemical techniques for fabricating and modifying semiconductors have recently begun to show promise as practical alternatives to high-vacuum techniques. In addition, the use of small band-gap semiconductors in photoelectrochemical devices is increasing. For these advances to continue a greater understanding of the processes occurring at the semiconductor/electrolyte interface on an atomic scale is necessary. *In situ* electrochemical STM and AFM offer the opportunity to gain new insight into the processes controlling both deposition and corrosion at semiconductor electrodes. The discrete energy levels in the semiconductor, however, complicate the use of STM for such studies, because tunneling is only possible in certain potential ranges where the energy of surplus electrons or holes in the semiconductor overlaps with appropriate states in the tunneling tip.[246] Already, though, a number of studies have been performed on GaAs, Si, NiP, and the transition metal chalcogenides. These studies indicate that the *in situ* SPM techniques are valuable tools for characterization of growing or corroding films and multilayers, as well as for confirming structural evidence deduced from other techniques.

A. Titanium Oxide

An early study by Itaya and Tomita indicated that *in situ* STM imaging of semiconductors under electrochemical conditions was possible on *n*-TiO_2 surfaces.[247] In order to attain stable tip−surface tunneling, they found it necessary to maintain the semiconductor surface polarized at a potential lower than the flat band potentials. Under these conditions they were able to obtain images of surfaces produced by two different chemical etching techniques. The surface created by etching in hot H_2SO_4 was observed to be smooth. The surface produced by etching in a solution of HNO_3/HF/CH_3COOH was found to be rougher, indicating that the etching procedure does not completely remove the damaged layer produced by mechanical polishing.

B. Zinc Oxide

The same authors performed related studies on *n*-ZnO_2 surface.[248] Under similar tunneling conditions to those used for *n*-TiO_2, they observed a rolling hill texture on *n*-ZnO samples prepared by etching in concentrated HCl. No significant change in the surface morphology was observed upon changes to the etching time.

C. Gallium Arsenide

In 1991, Eriksson et al. presented images of *n*-GaAs(100) surfaces in alkaline solution taken with the STM.[249] Careful selection of sample potential allowed them to obtain images during anodic polarization of the semiconductor, under which conditions, GaAs undergoes photocorrosion when illuminated. The images indicated that the initially smooth electrode surface roughens as the photocorrosion process proceeds.

Later, Uosaki's group used the AFM to image *n*-GaAs(100)[250] and *p*-GaAs(111)[251] in aqueous HCl. In this environment, they found that the *n*-GaAs(100) surface was smoothed at anodic potentials under illumination. On *p*-GaAs(111), they observed that uniform 50−100 nm structures were formed at open circuit, which they ascribed to a small current which is compensated by the photocurrent. At more anodic potentials, they observed further formation of these structures which they ascribe to etching by the anodic photocurrent. On both the *n*- and *p*-type GaAs, they observed no change in the surface structure at cathodic potentials where no current flows. In addition, they were able to take atomic resolution images revealing the expected (1×1) surface lattices at these more cathodic potentials. In further work,[252] they point out that the electrochemical characteristics of the electrode are altered when the surface has been exposed to sufficient anodic polarization to induce structural changes.

Yao et al. have investigated the behavior of *n*-GaAs(111) in sulfuric acid solution with the STM.[253] The semiconductor electrodes were chemically etched with a procedure expected to result in a Ga-terminated surface. Atomic resolution STM images ob-

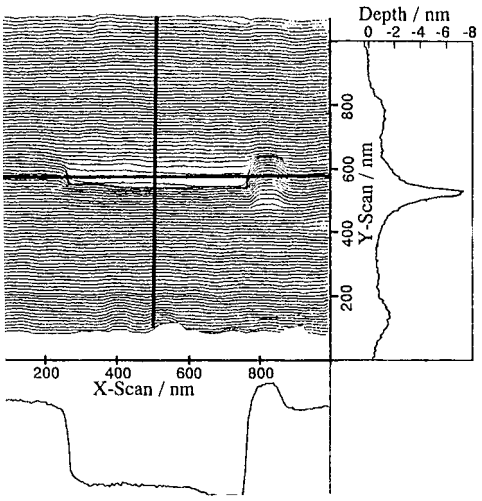

Figure 14. AFM image (1000 × 1000 nm) of a *p*-GaAs surface in 10 mM H_2SO_4 at the open-circuit potential after only the *x* direction was scanned for 30 min with stronger force. Sectional views corresponding to the thick solid lines in the image are also shown. (Reprinted with permission from ref 256. Copyright 1996 Elsevier Science.)

tained at cathodic potentials revealed the hexagonal symmetry and 4 Å interatomic spacing expected from the Ga-terminated (111) face. Longer range images showed steps of height consistent with the two-layer spacing between Ga layers in the semiconductor and terrace edges that intersected at the 60° and 120° angles expected for the (111) face. These results confirmed that the chemical etching technique used did in fact result in a well-ordered Ga-terminated surface. Similar work also revealed the expected (1×1) structure on *n*-GaAs(001).[254]

Uosaki also studied the electrodeposition of Sn on *n*-GaAs for possible use as a conducting, protective film on the electrodes in photoelectrochemical devices.[255] While Sn is not an ideal metal for such coatings, it was chosen because it undergoes deposition in a potential region where the *n*-GaAs provides stable tunneling for imaging. In alkaline solution they found that distinct features nucleated and grew at low deposition overpotentials. At larger overpotentials and current densities deposition occurs over a larger portion of the surface and growth of large discrete features is less pronounced. In acidic solution at low overpotentials, they found that the deposited surface was even rougher than in alkaline solution under similar conditions.

In other work, they have studied AFM enhanced dissolution and deposition on *p*-GaAs(100) electrodes.[256] They found that photoelectrochemical etching at anodic potentials was enhanced in regions which were scanned with the AFM tip. Scanning in only one direction produced trenches which imaged the shape of the AFM tip, as shown in Figure 14. No dissolution was observed when the surface was scanned at cathodic potentials where photocorrosion of the electrode does not normally occur. A similar enhancement was observed for Cu deposition on the electrode at cathodic potential, resulting in selective deposition on areas which were scanned with the AFM, especially when the scan area was greater than 500 × 500 nm.

D. Silicon

Bockris and co-workers used the STM to investigate the surface state of *p*-Si(111) in the electrochemical environment in 1991.[257] They performed their experiments in propylene carbonate solution to minimize faradaic interference with the tunneling current under the extreme bias voltages required at the STM tip. They found that at negative electrochemical potentials and bias voltages between −0.6 and 0.4 V tunneling was not sufficient to reveal surface features on the electrode. At positive electrochemical potentials, images were only obtained when the bias voltage exceeded 2.2 V. They assigned the onset of tunneling in the band gap region to the presence of surface states created by adsorbed solvent or ionic species. It was noted that the tunneling biases required to support imaging were different in solution from those required in air.

The etching of *n*-Si(111) in alkaline solutions was studied with the STM by Allongue et al.[258] They found that at potentials where hydrogen evolution occurs, Si dissolution occurs primarily a step flow mechanism along the (110) direction, as shown in Figure 15. This resulted in formation of smoother step edges. Etching at more anodic potentials resulted in more rapid dissolution of the Si surface, and formation of pits in the middle of terraces.

Itaya et al. have studied the etching of *n*-Si(111) in F^- containing electrolyte with the STM.[259] Their experiments were performed in the dark to minimize the effect of photoinduced corrosion, and at cathodic potentials to minimize electrochemical dissolution. They were able to achieve atomic resolution images of the H terminated Si(111) (1×1) surface. The etching of the surface was found to proceed in a primarily layer-by-layer fashion. Etching was fastest at steps containing kink sites. They attributed this enhanced etching rate to higher reactivity of the dihydrogen terminated Si atoms present at kink sites relative to the monohydrogen terminated Si found at other step edges. In similar work on the (001)[260] and (110)[261] faces of *n*-Si, also revealed the H terminated (1×1) lattice. Smoothing of these surfaces was found to occur in a layer by layer fasion with dissolution fastest at steps and kinks.

Bockris and co-workers have used the STM to investigate the photoelectrochemical plating of Pt on *p*-Si(111) electrodes.[262] Their experiments indicated that a rougher Pt deposit is obtained when the reduction is carried out under illumination than when the deposition is performed in the dark. They interpret this difference as indicating that Pt crystal growth is favored in the dark where electrons leave the electrode through surface states at low overpotentials. In the light, they claim that nucleation is favored due to the high overpotentials generated by first promoting the electrons to the conduction band from which they are transferred to the electroactive species in solution.

E. Cadmium Sulfide

In 1991, Zhao et al. used the STM to study electrochemical and photoelectrochemical corrosion of CdS particles in KCl solutions.[263] Approximately

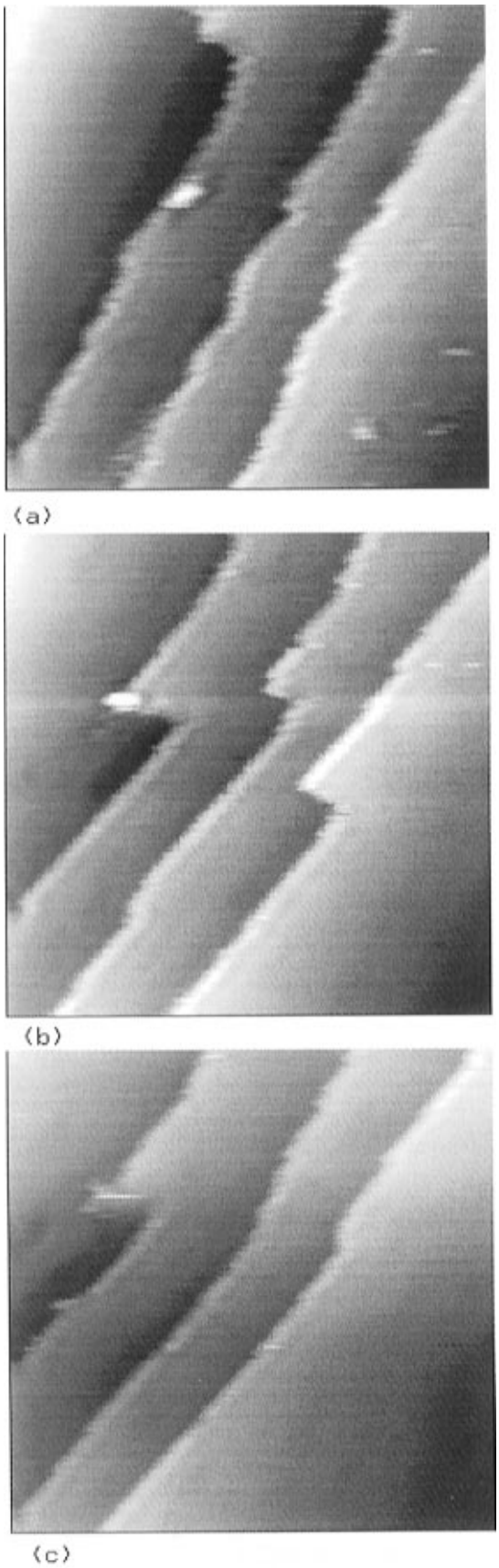

Figure 15. Sequence of STM images showing the evolution of step edges on an *n*-Si(111) surface in contact with 2 M NaOH. The (380 × 380 Å) images (a−c) have been recorded in 45 s. The time elapsed between images is 90 s. Tunneling conditions: sample, $U_S = -0.63$ V/Pd-H, $I_S = -150$ μA/cm^2; tip, $U_T = +300$ mV/Pd-H, $I_T = 0.2$ nA. (Reprinted with permission from ref 258. Copyright 1992 Elsevier Science.)

300 Å thick layers of CdS particles supported on HOPG were observed to be etched during cathodic potential scans from 0 V vs Ag/AgCl in the dark. Three such scans yielded a noticeable decrease in grain size. After 10 excursions, the flat HOPG substrate was observed between the remaining rough islands of CdS particles. Illumination of the supported particles at 0 V resulted in photocorrosion which could be observed with the STM as migration and increasing inability to distinguish individual particles. Illumination at an anodic potential of 1.2 V led to an accelerated corrosion process and almost complete removal of CdS from the HOPG surface.

More recently, Demir and Shannon have studied the electrochemical growth of CdS, using the STM to characterize the initial stages of growth *in situ*.[264] They employed a layer by layer growth technique in which they first adsorbed a monolayer of S^{2-} to Au(111) electrodes from Na_2S solution. Images taken at potentials where the adlayer was stable indicated the formation of a $(\sqrt{3}\times\sqrt{3})$R30° S lattice. Subsequent cathodic deposition of Cd^{2+} yielded an atomically flat structure. Atomic resolution images evinced a hexagonal (3×3) structure which they believe to be strongly influenced by epitaxial deposition on the Au(111) substrate.

F. Molybdenum Disulfide

Molybdenum disulfide has received much attention as a potential material for photoelectrochemical energy conversion due to its relative resistance to photoelectrochemical corrosion relative to other semiconductors. Sakamaki et al. have studied the mechanism of photocorrosion on (0001) faces of *n*-MoS_2 in CH_3CN solutions using the STM.[265] They found that atomically flat terraces of the material were stable at anodic potentials under illumination. Under these conditions, some dissolution was observed at defect sites. However, the addition of small amounts of H_2O to the solution (∼4%) greatly increased the dissolution at defect sites, as seen in Figure 16. In further work,[266] they observed that under these conditions small defects grew into triangular pits which reflected the crystallographic symmetry of the semiconductor crystal.

G. Lead Sulfide

Higgins and Hamers have used the STM to study both the anodic and cathodic dissolution of PbS(001) in aqueous solutions.[267] At potentials more anodic than the open circuit potential, they observed enhanced etching at step edges and nucleation of monolayer deep pits at sites believed to originally be impurities. At moderate cathodic potentials, small protrusions were observed to grow on the surface, which they attributed to an underpotential deposition process involving reduction of Pb^{2+} to Pb^0 on the surface. At more extreme cathodic potentials, drastic surface changes were observed due to the bulk reduction of lead. The material required for formation of the lead islands at moderate potentials is observed to come from dissolution at step edges. Atomic resolution images revealed the expected square (001) surface lattice. Atomic resolution of the

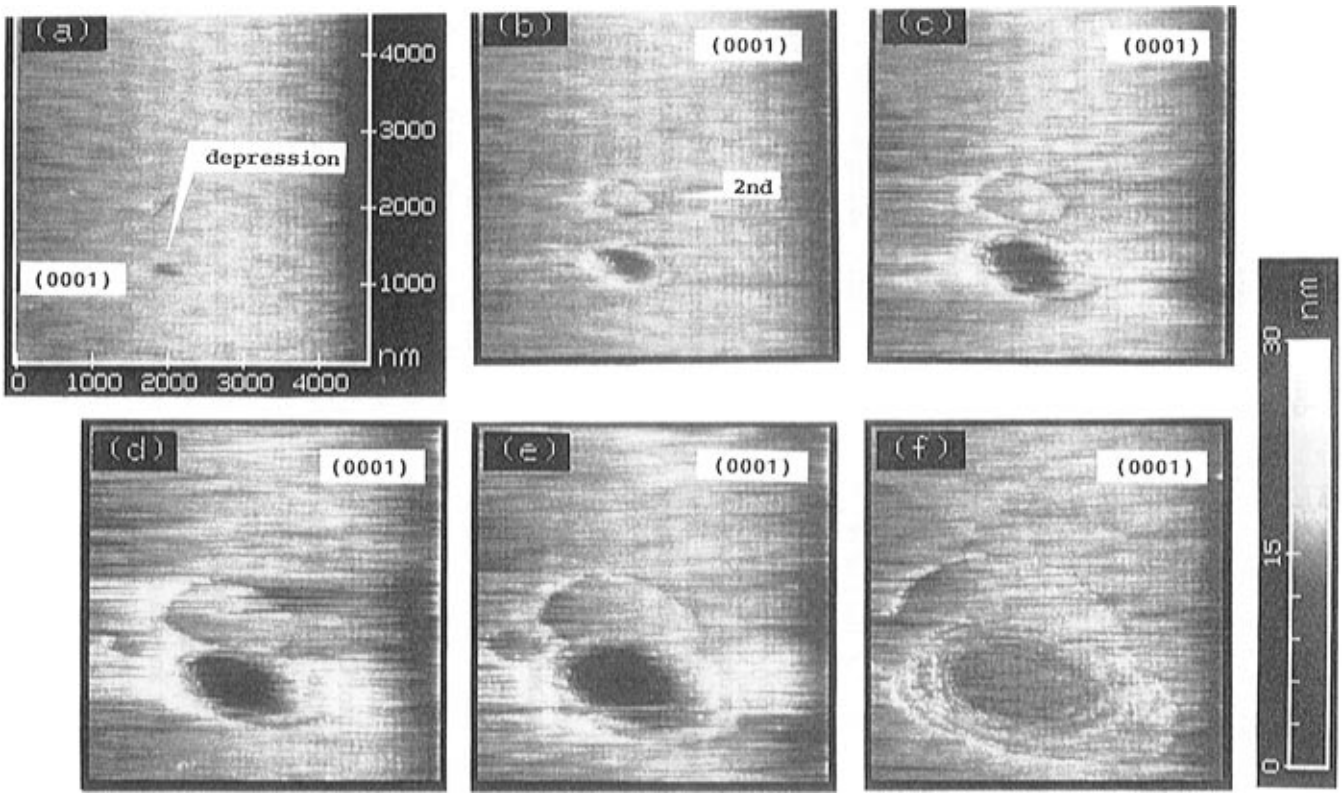

Figure 16. Dynamically morphological transformations of n-MoS_2 surface obtained by adding 4 vol % H_2O to CH_3CN under photoelectrochemical control. All images were obtained in a constant current mode (5.3 nA) at $T_B = 600$ mV (WE/tip(ground)), $E_w = +0.7$ V vs SCE, and $E_T = +0.1$ V vs SCE. The scanning area was 4500 × 4500 nm: (a) observed in CH_3CN/10 mM TBAP; (b, c, d, e, and f) imaged after 10, 21, 31, 41, 61 s, respectively, following the addition of 4 vol % H_2O to the solution used in a. (Reprinted with permission from ref 265. Elsevier Science.)

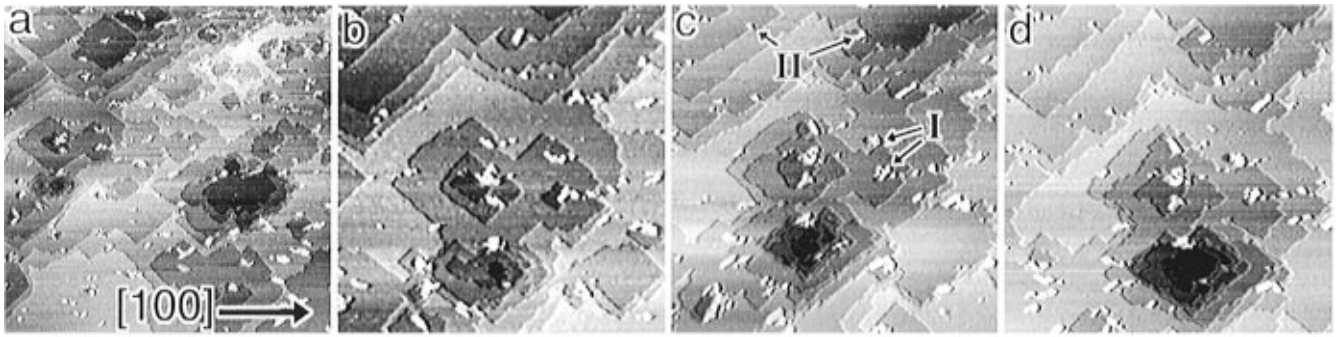

Figure 17. Real-time sequence of STM images of the galena(001) surface showing the dissolution process. (a) 6250 × 6250 Å image; (b−d) 2000 × 2000 Å images. The time to acquire each image was approximately 3 min. (Reprinted with permission from ref 268. Copyright 1996 American Vacuum Society.)

tops of the deposited lead islands showed a hexagonal structure indicative of a preferential Pb(111) deposition geometry.

In further work, they used the STM to observe single atom vacancies on the PbS surface and to study the effect of Cl^- ions on surface morphology.[268] In these studies they also observed that the step edges were primarily oriented perpendicular to the (110) surface directions, as shown in Figure 17. This is contrasted with the situation in vacuum where such edges are electrostatically unfavorable. They found that the dissolution of the surface is ordinarily slow and occurs at step edges at potentials near the open circuit potential. The addition of Cl^-, however, results in the nucleation of dissolution pits on the surface.

H. Indium Selenide

Uosaki and Koinuma used the AFM to study the surface state of InSe during anodic polarization.[269] They found that the hexagonal InSe surface structure was observable at cathodic potentials. Images taken while scanning the electrode potential to more anodic values showed an increasing lack of atomic resolution, finally resulting in the appearance of an amorphous surface. These images were attributed to the formation of an amorphous Se layer at anodic potentials. Scanning the potential back to the cathodic region resulted in the reappearance of atomic order in the images, indicating that the original surface state had been restored.

I. Nickel Phosphide

Homma et al. have used *in situ* STM to study the differing morphologies of electroless and electrochemically deposited NiP films.[270] The electroless films were observed to form from many nucleation sites over the surface of the HOPG substrate. The resulting films had a rough surface texture at the end of deposition. Electrolytically deposited films generally formed large grains which spread smoothly across the surface. The resulting surface morphology consisted of wider grains with smooth domelike tops.

Wouters et al. studied the electrochemical deposition of Sn on NiP films in the presence of various organic additives to determine the effect of the additives on the film morphology.[271] The primary focus of this work was to correlate the electrochemical potential characteristics of the pulsed current deposition procedure with the surface state. While no additives were found that provided adequate Sn films, a strong correspondence was found between the voltammetry and the AFM images. The presence of a voltage plateau at a smaller overpotential in the early stages of deposition which gives way to a higher deposition overpotential at later times was clearly correlated with a rough surface texture indicative of a nucleation growth mechanism. The change in potential is ascribed to the different energetics of depositing tin on an isolated cluster supported on NiP vs depositing tin on the continuous film that is formed after the nucleated islands coalesce.

IX. Molecular Adsorbates on Electrode Surfaces

Perhaps the most exciting and certainly the least well-developed area in the convergence of electrochemistry and SPM is that involving study of the structure and reactivity of more complex adsorbates on electrode surfaces. This area is significant because of the importance of molecular adsorbates in areas as diverse as corrosion protection, deposition, catalysis, and structural modification. There is a natural correspondence here between work performed in UHV and work in solution. Early efforts directed at imaging organic molecules on surfaces were hampered by ill-defined surface chemistry and agglomeration of adsorbates. However, within the past few years, several groups have reported images of a variety of adsorbates on electrode surfaces. Because the diversity of organic and inorganic adsorbates is so large and because molecular transformations are crucial to devices as important as sensors and fuel cells, these studies will continue to have importance for some time to come.

A. Alkanethiols

Some of the most commonly used adsorbates in surface science are alkanethiols, the structure and reactivity of which have been the focus of attention for well over a decade.[272] Most SPM studies of this material have been carried out in the air ambient or UHV environments, but there are a few studies in solution. Pan, Tao, and Lindsay[273] used the AFM to show that these materials exhibit the same $(\sqrt{3}\times\sqrt{3})$-R30° structure in solution as they do in air. Another thiol moiety-containing adsorbate—L-cysteine—also forms a $(\sqrt{3}\times\sqrt{3})$R30° adlayer structure.[274] However, isothiocyanoporphyrin forms only a disordered structure on a Au(111) surface following deposition from mesitylene.[275] Penner and co-workers[276] used the STM to examine tunneling through a freshly formed alkanethiolate layer atop newly deposited Ag "nanodisk" structures. The change in apparent height of the Ag crystallites increased linearly with the length of the thiol and equaled the expected all-trans chain length of these molecules. These data suggest that the STM tip penetrates only minimally into the thiol monolayer, a result different from what was inferred in *ex situ* measurements.

B. Carbon Monoxide

The first study of CO binding to Pt(111) surfaces was by Ito who reported four potential-dependent structures of this adsorbate.[277] At low coverage, these authors observed the $(\sqrt{3}\times\sqrt{3})$R30° found previously in UHV. However, at high coverage, they observed compression structures of CO which were different from those observed in UHV. Villegas et al. studied the adsorption of CO on Pt(111) with the STM in greater detail and observed similar behavior to that seen in the CN^- system.[278] At low potentials in CO saturated solution, they observe a (2×2)-3CO overlayer with CO molecules bound in both atop and bridging sites. This structure has a coverage of 0.75 ML. At more positive potentials they observe a $(\sqrt{19}\times\sqrt{19})$R23.4°-13CO adlayer with a coverage of 0.685 ML, which is shown in Figure 18. Like the CN^- system, this structure consists of CO molecules in atop sites surrounded by molecules which are not adsorbed specifically at atop, 2-fold, or 3-fold sites. In this case the arrangement gives rise to a moiré pattern instead of clusters on the surface. In both of these structures, the STM data was complemented by surface IR data which confirmed the existence of nonequivalent binding sites within the adlayer. In solutions that were purged of CO after adsorption was allowed to take place, they observed a less dense $(\sqrt{7}\times\sqrt{7})$R19.1°-4CO structure. On Pt(100), Vitus et al. observed islands of a (1×1) CO overlayer which were found to coalesce as the electrode potential was increased.[279]

They observed yet another structure on Pt(111) electrodes predosed with Bi.[280] The surface was electrochemically dosed with 0.21 ML of Bi before the addition of CO. Dark regions of the image contained the potential dependent CO adlayers discussed above. The majority of the surface (ca. 70%) was covered with a $(3\times\sqrt{3})$ layer of mixed Bi and CO. This adlayer structure has important catalytic consequences.

Yau et al. have used STM and surface IR to record similar behavior on Rh(111) electrodes.[281] At high potentials they observe a (2×2)-3CO adlayer in which the adsorbed CO molecules cluster in groups of three within the lattice. This structure has a coverage of 0.75 ML. At lower potentials, they imaged a $(3\times\sqrt{3})$-4CO adlayer with a coverage of 0.67 ML. The presence of multiple binding sites in both structures was confirmed by *in situ* surface IR spectroscopy. On Rh(110), the Weaver group observed a (4×3)-12CO adlayer.[282]

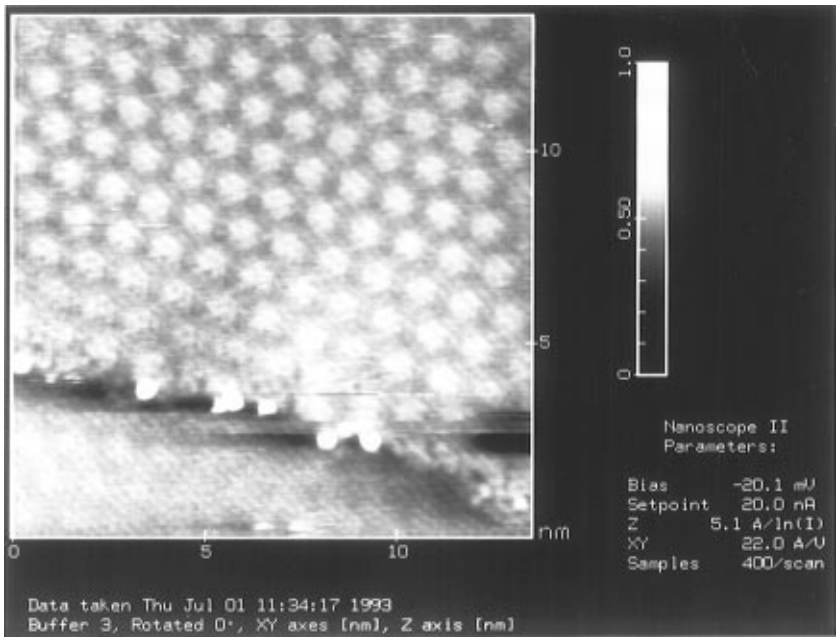

Figure 18. Constant height STM image of the Pt(111) ($\sqrt{19}\times\sqrt{19}$)R23.4°-13CO adlayer obtained in a CO saturated 0.1 M $HClO_4$ solution at 0.10 V vs SCE. (Reprinted with permission from ref 278. Copyright 1995 Elsevier Science.)

C. DNA Bases and Related Molecules

A number of studies have examined DNA bases and related adsorbates on HOPG and Au in solution. The earliest studies by Srinivasan and co-workers, revealed several different ordered structures of adenine[283] and guanine[284] on HOPG. Tao et al. examined the structure of all four DNA bases on Au(111) in $NaClO_4$.[285,286] In contrast to the behavior found on graphite, these authors showed that adenine and guanine formed polymeric aggregates in which the bases stacked with repeat distances reminiscent of double stranded DNA. Later work by Tao and Shi[287] examined the kinetics of dissolution of adenine and guanine films on HOPG and compared structures as revealed by both AFM and STM. In the case of both molecules, the STM images exhibited higher resolution and revealed a convolution of the electronic structure of the surface and the adsorbate. This convolution was described in more detail in a later publication, which also examined the tip induced distortion of the graphite−guanine molecule interface.[288] Tao and Shi also showed in other work that oxidative dissolution of guanine is initiated preferentially from line defects[289] a behavior they also observed with xanthine.[290]

Because of their complexity relative to simpler adsorbates, organic molecules can exhibit more involved behaviors on electrode surfaces. One example of this complexity is the order−disorder transition observed in 2,2′-bipyridine on Au(111).[291] At positive potentials where there is positive charge on the electrode surface, the bipyridine molecule stands vertically on the surface and forms polymeric chains, as shown in Figure 19. With low surface charges, the chains are randomly oriented, but they begin to align as the charge density reaches a critical value. The transition from disordered to ordered starts with the appearance and then the coalescence of small ordered domains.

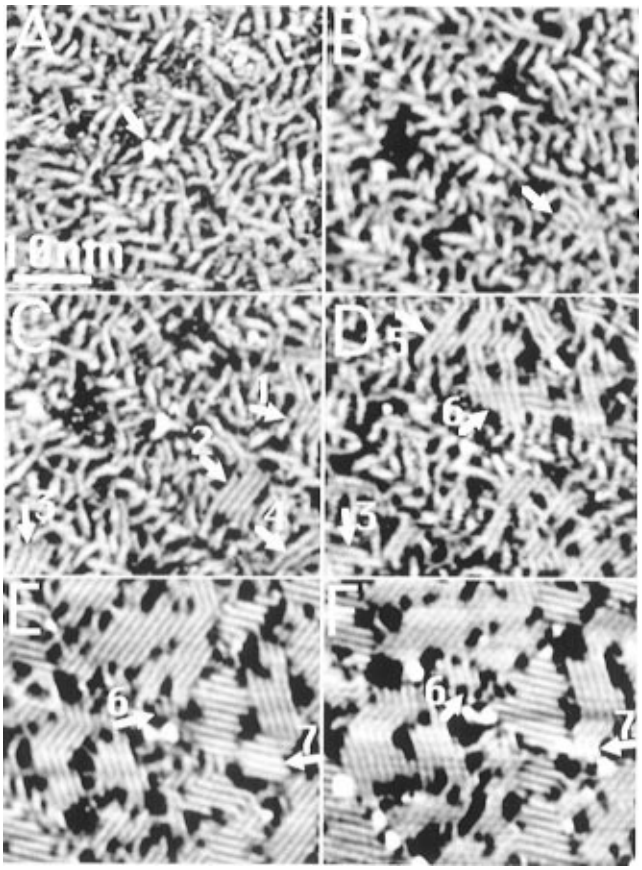

Figure 19. STM images of surface charge induced transition from disordered to ordered phases in 2,2′-bipyridine monolayer. Surface potential was increased from −0.1 V vs SCE (image A) to 0.4 V vs SCE (image F). Arrows (1−7) indicate domains of ordered bipyridine molecules. (Reprinted with permission from ref 291. Copyright 1995 American Physical Society.)

There has also been examination of molecules whose behavior is even more complex on Au(111). Examples include thymine,[292] cytosine,[293] and uracil[294,295] where an attempted correlation between

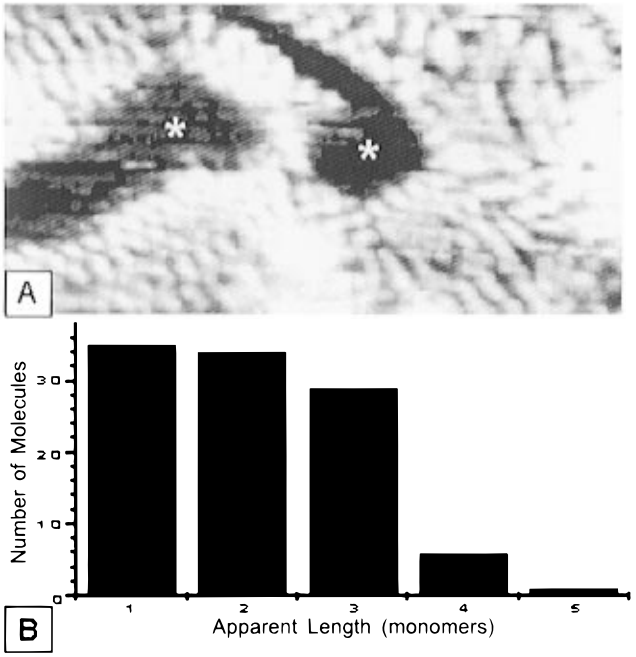

Figure 20. (A) A 10 × 20 nm STM image of oligomers on Au(111) at +340 mV vs NHE, following the electrooxidation of phenoxide by sweeping the potential to +600 mV. Molecule width is 0.72 ± 0.1 nm and length varies from 0.8 to 2.5 nm. I_{tip} = 2 nA. E_{tip} = 355 mV. (B) Bar graph depicting the distribution of oligomer lengths in A. (Reprinted with permission from ref 297. Copyright 1995 American Chemical Society.)

electrochemical and capacitive behavior and *in situ* STM images was carried out. In both cases, the capacitance measurements indicate that these molecules possess both "chemisorbed" and "physisorbed" states on the surface, the existence of which can be controlled by the applied potential. An interesting study by Bunge et al.[296] examined the structure of tetramethylthiourea—a molecule noteworthy for its use as a Cu-plating additive—on Au(111). The tetramethylthiourea was observed to form a (3×3) structure and catalyzed the slow dissolution of the Au surface at potentials prior to its desorption from the electrode.

D. Phenol, Pyrrole, and Aniline

The STM has been used monitor the electrooxidation of phenoxide to oligophenol on Au(111) in alkaline solutions.[297] Prior to oxidation, phenol associates as phenoxide to Au(111) in a $(\sqrt{3}\times\sqrt{3})R30°$ structure with the molecule oriented end-on through the O atom. The presence of order in this array is a function of the substitution on the phenol ring.[298] After oxidation, which is initiated at step edges and other defects,[299] a disordered, close-packed array of oxidation products consisting of monomers, dimers, trimers, and a few higher lengths are observed (Figure 20). The oxidation products are oriented with the ring roughly parallel to the electrode surface. These results show one of the transformations that organic molecules can undergo on electrode surfaces. Phenol oxidation has also been studied on HOPG.[300]

A few groups have examined the electrodeposition and polymerization of larger systems *in situ*. Examples include the deposition of polypyrrole[301] where the STM tip was used to control the sites of deposition and the polymerization of aniline.[302] Observation of the evolution of the structure of polymethylthiophene has also been performed.[303]

E. Porphyrins

Porphyrins and related molecules form another class of molecules imaged on surfaces in the electrochemical environment. Iron(III) and Zinc(II) protoporphyrin(IX) both form identical ordered arrays when adsorbed on HOPG from aqueous solution.[304] These arrays are essentially those formed by close packing the molecules into a two-dimensional layer. The molecules with different metals can be distinguished from each other by their different internal structure. The different internal structure formed the basis for a more involved discussion[305] about the role of orbitals near the Fermi level in enhancing the tunneling probability; molecules containing the redox-active Fe center exhibit tunable tunneling currents in a manner much different from the free base form of protoporphyrin (IX).

Molecular adsorption on HOPG has the potential to be problematic due to the ease of compressibility of the graphite layers. Itaya and co-workers have developed an effective system with which to immobilize porphyrin and related centers by adsorption onto I-modified surfaces. In their initial work,[306] they demonstrated that a specific modified porphyrin formed ordered arrays on Au(111)-I. The same ordering procedure was found on Ag(111)-I surfaces, where considerable internal detail in the porphyrin molecule was resolved[307] and rows of crystal violet were imaged, as seen in Figure 21.[308]

F. Benzene

One of the first triumphs of STM imaging in UHV was the resolution of the (3×3) adlayer structure of benzene coadsorbed with CO on Rh(111).[309] This series of images underscored the utility of STM to study adsorbates on surfaces. Recently Itaya and coworkers showed that very similar structures were formed on Rh(111) in HF solution, although without the presence of CO (Figure 22).[310] The authors speculated that the stabilizing CO in UHV was replaced by water or hydronium binding to uncoordinated Rh. In the same paper, this group reported several other benzene structures on both Rh(111) and Pt(111). The images were interpreted as arising from benzene adsorbed on 2-fold bridging sites on these surfaces and transformations between different specific arrangements were imaged. The high quality of these images and their coincidence and extension of the UHV work performed some eight years earlier bodes well for future work studying adsorbates on electrode surfaces in solution.

G. Polyoxometalates

Only one report of an *in situ* image of an inorganic adsorbate (other than the small anions discussed above) appears in the literature.[311] STM images indicate a $c(5\times3\sqrt{3})$ structure formed by the self-assembly of α-dodecatungstosilic acid, α-$H_4SiW_{12}O_{40}$, which spontaneously forms adherent, passivating,

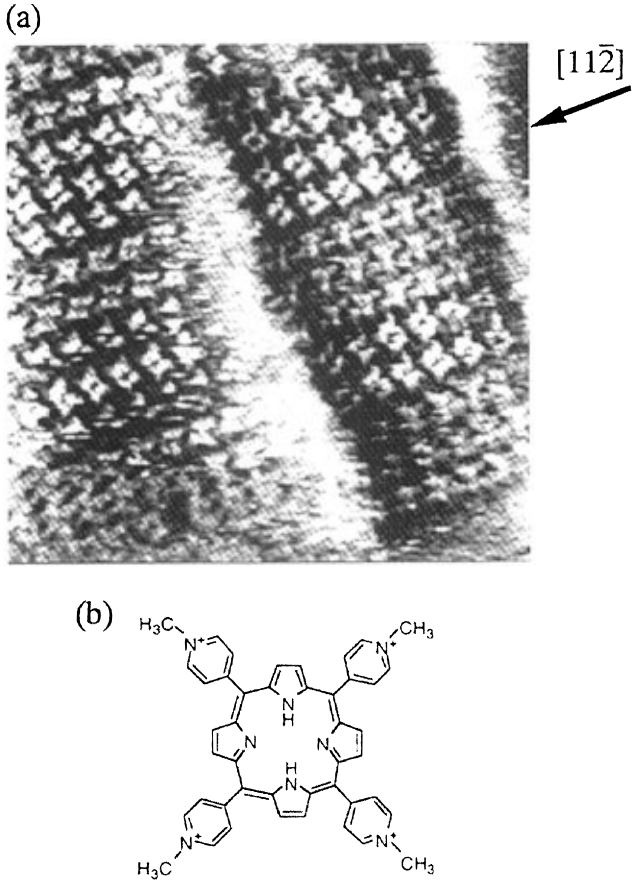

Figure 21. STM image of a porphyrin adsorbed on I on Ag(111). (Reprinted with permission from ref 307. Copyright 1996 American Chemical Society.)

monolayer-thick, ordered molecular arrays on Ag(111) surfaces upon immersion of the surfaces into an aqueous solution of the acid. These monolayers form a nearly square adlattice on this surface, the structure of which is derives from the square template of the molecule itself.

X. Conclusions

The work described in this review shows very strongly that over the last five years an exponential advance in our understanding of the structure and reactivity of electrode surfaces has occurred. In areas as diverse as surface reconstruction, oxide formation, small molecule adsorption, corrosion, and deposition, probe microscopy has had a substantial impact.

Observation of the reconstruction of the low Miller index faces of Au was one of the triumphs of *in situ* STM. While these rearrangements had been inferred from optical and voltammetric studies, direct visualization of the structures and development of understanding of ways to control these rearrangements has been unprecedented. These studies are part of an overall effort to understand the electrochemical double layer and to correlate the detailed structure of the electrode surface with the double-layer structure and ultimately with electrochemical response.

Studies of ionic adsorption are prosecuted in this same vein. Of particular note in this area is the direct visualization of anions such as sulfate on the electrode. While complete understanding of these images remains for the future, the anions themselves

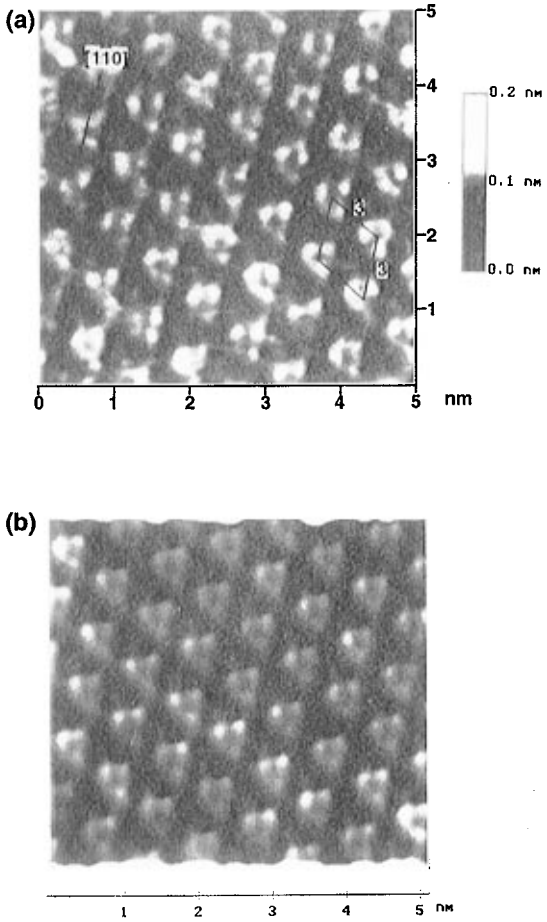

Figure 22. Unfiltered top view (a) and height-shaded plot (b) of the Rh(111)-(3×3)-1C_6H_6 adlattice acquired at 0.25 V in 0.05 mM benzene and 0.01 M HF. The bias voltage and feed back current were set at 30 mV and 20 nA. (Reprinted with permission from ref 310. Copyright 1996 American Chemical Society.)

constitute the inner Helmholtz plane and their observation is quite significant. Developing an understanding of the double layer and ways in which it can be controlled and modified will continue to be an important task for the future in nonaqueous as well as the aqueous environments considered thus far.

Fundamental studies of the reactivity of semiconductor surfaces are also just beginning. The scanning probe microscopies have allowed direct observation of semiconductor surface morphology after treatment by various etching procedures. This will continue to be an important application of SPM as more and better preparation techniques are devised. In addition, as use of semiconductors in photoelectrochemical devices increases, the ability of STM and AFM to directly probe the changes occurring during corrosion of the semiconductor and deposition of protective layers will become invaluable.

Scanning probe microscope studies of the upd process have revealed a rich structural and reactive chemistry on a variety of substrates, the detailed nature of which is dependent on potential, available anions, substrate orientation, and substrate identity. Several different structural motifs have been identified including: commensurate monolayers stabilized by coadsorbed anions, close-packed incommensurate monolayers, open monolayers which are commensu-

rate in only one direction, and finally, an open linear structure. As emphasized above, the upd work in particular has benefited from complementary studies, especially by the SXS technique, due to the facile scattering present off of the relatively heavy upd adatom. A detailed, general, predictive theory of upd structure and behavior is not yet forthcoming. Undoubtedly, continued effort using probe microscopy will attend these interesting systems.

There is considerably less clarity in the area of bulk deposition because of the complexity of this process. Metal plating is clearly affected by the presence of defects and other inhomogeneities on the surface. Moreover, there is an overarching interaction with plating additives through which the deposit texture is strongly affected. Fundamental questions concerning the nature of the interaction between the additive, the surface, and the adatom remain to be addressed. Questions about site bias for deposition and the interplay of this bias with solution and electrochemical conditions are equally important. The connection between a microscopic description of deposition and the ultimate texture of the deposit will also have to be clarified. Corrosion is an even more complex process, the study of which at a microscopic level with probe microscopy is only just starting.

A very important and encouraging development in SPM studies of electrodes is the recent emphasis on studying the structure and activity of larger molecules on surfaces. These studies address the reactivity of molecules on surfaces—reactivity important in a wide variety of areas including energy production, deposition, and corrosion protection—and also address more fundamental issues relating to the electron transfer event through these molecules which, among other areas, has biological implications. Continued development along this line will be quite significant.

But more importantly, modification of surfaces with molecules provides a way to control the structure and reactivity of the surface to obtain new properties. As we understand more about the structure of surfaces and what nature presents, we will undoubtedly develop new ways of changing the surface. Inorganic chemistry was greatly enlivened in the early 1960s through the routine use of structure-determining tools such as X-ray crystallography and NMR spectroscopy. Once the product of reactions could be understood, they could be controlled. Surface electrochemists now possess nearly equivalent tools, namely the probe microscopes, and it is nearly certain that the next decade will see many more important developments.

XI. Acknowledgments

A.A.G. thanks his students and co-workers for their contributions over the last nine years. Work by the authors described in this review was funded by the Department of Energy through the Frederick Seitz Materials Research Laboratory at the University of Illinois (DE-FG02-91ER45349).

XII. References

(1) Soriaga, M. P. *Prog. Surf. Sci.* **1992**, *39*, 325.
(2) Wagner, F. T. *In Structure of Electrified Interfaces*; Lipkowski, J., Ross, P. N., Eds.; VCH: New York, 1993; pp 309−400.
(3) Sonnenfeld, R.; Hansma, P. K. *Science* **1986**, *232*, 211.
(4) Liu, H. Y.; Fan, F. R.; Lin, C. W. *J. Am. Chem. Soc.* **1986**, *108*, 3838.
(5) Wiechers, J.; Twomey, T.; Kolb, D. M.; Behm, R. J. *J. Electroanal. Chem. Interfacial Electrochem.* **1988**, *248*, 451−460.
(6) Lustenberger, P.; Rohrer, H.; Christoph, R.; Siegenthaler, H. *J. Electroanal. Chem.* **1988**, *243*, 225.
(7) Itaya, K.; Tomita, E. *Surf. Sci.* **1988**, *201*, L507−L512.
(8) Gewirth, A. A.; Bard, A. J. *J. Phys. Chem.* **1988**, *92*, 5563−6.
(9) Yau, S.-L.; Vitus, C. M.; Schardt, B. C. *J. Am. Chem. Soc.* **1990**, *112*, 3677−3679.
(10) Magnussen, O. M.; Hotlos, J.; Nichols, R. J.; Kolb, D. M. *Phys. Rev. Lett.* **1990**, *63*, 2929.
(11) Binnig, G.; Rohrer, H.; Gerber, C.; Weibel, E. *Phys. Rev. Lett.* **1989**, *49*, 57.
(12) Chen, C. J. *Introduction to Scanning Tunneling Microscopy*; Oxford Series in Optical and Imaging Sciences; Oxford University Press: New York, 1993.
(13) Bonnell, D. A. Ed. *Scanning Tunneling Microscopy and Spectroscopy: Theory, Techniques, and Applications*; VCH: New York, 1993.
(14) Güntherodt, H.-J., Wiesendanger, R., Eds. *Scanning Tunneling Microscopy I: General Principles and Applications to Clean and Adsorbate-Covered Surfaces*; Springer Series in Surface Sciences; Springer-Verlag: Berlin, 1992; Vol. 20.
(15) Wiesendanger, R.; Güntherodt, H.-J. *Scanning Tunneling Microscopy II: Further Applications and Related Scanning Techniques*; Springer Series in Surface Sciences; Springer-Verlag: Berlin, 1992; Vol. 28.
(16) Wiesendanger, R.; Güntherodt, H.-J., Eds. *Scanning Tunneling Microscopy III: Theory of STM and Related Scanning Probe Methods*; Springer Series in Surface Sciences Springer-Verlag: Berlin, 1993; Vol. 29.
(17) Magonov, S. N.; Whangbo, M. *Surface Analysis with STM and AFM: Experimental and Theoretical Aspects of Image Analysis*; VCH: New York, 1996.
(18) Clavilier, J.; Faure, R.; Guinet, G.; Durand, R. *J. Electroanal. Chem.* **1980**, *107*, 205.
(19) For a review, see: Hamelin, A. *J. Electroanal. Chem.* **1996**, *407*, 1.
(20) Binnig, G.; Quate, C. F.; Gerber, C. *Phys. Rev. Lett.* **1986**, *12*, 930.
(21) Manne, S.; Butt, H.-J.; Gould, S. A. C.; Hansma, P. K. *Appl. Phys. Lett.* **1990**, *56*, 1758.
(22) Manne, S.; Hansma, P. K.; Massie, J.; Elings, V. B.; Gewirth, A. A. *Science* **1991**, *251*, 183−186.
(23) Cataldi, T. R. I.; Blackham, I. G.; Briggs, G. A. D.; Pethica, J. B.; Hill, H. A. O. *J. Electroanal. Chem. Interfacial Electrochem.* **1990**, *290*, 1−20.
(24) Arvia, A. J. *Surf. Sci.* **1987**, *181*, 78−91.
(25) Kolb, D. M.; Nichols, R. J.; Behm, R. J. In *Electrified Interfaces in Physics, Chemistry and Biology*; NATO ASI Series C; Kluwer Academic: Dordrecht, 1992; Vol. 355, pp 275−292.
(26) Siegenthaler, H.; Christoph, R. In *Scanning Tunneling Microscopy and Related Methods*; Behm, R. J.; Garcia, N.; Rohrer, H., Eds.; NATO ASI Series E; Kluwer Academic: Dordrecht, 1990; Vol. 184, pp 315−333.
(27) Christensen, P. A. *Chem. Soc. Rev.* **1992**, *21*, 197−208.
(28) Sonnenfeld, R.; Schneir, J.; Hansma, P. K. *Mod. Aspects Electrochem.* **1990**, *21*, 1−28.
(29) Siegenthaler, H. In *Scanning Tunneling Microscopy II*; Wiesendanger, R., Güntherodt, H.-J., Eds.; Springer Series in Surface Sciences; Springer-Verlag: Berlin, 1992; Vol. 28, pp 7−49.
(30) Weaver, M. J.; Gao, X. P. *Annu. Rev. Phys. Chem.* **1993**, *44*, 459.
(31) Weaver, M. J. *J. Phys. Chem.* **1996**, *100*, 13079−13089.
(32) Bard, A. J.; Abruna, H. D.; Chidsey, C. E. D.; Faulkner, L. R.; Feldberg, S. W.; Itaya, K.; Majda, M.; Melroy, O.; Murray, R. W.; Porter, M. D.; Soriaga, M. P.; White, H. S. *J. Phys. Chem.* **1993**, *97*, 7147−7173.
(33) Gewirth, A. A., Siegenthaler, H., Eds. *Nanoscale Probes of the Solid/Liquid Interface*; NATO ASI Series E: Applied Sciences Kluwer Academic: Dordrecht, 1995, Vol. 288.
(34) Toney, M. F.; Melroy, O. R. In *Electrochemical Interfaces: Modern Techniques for In-Situ Interface Characterization*; Abruna, H. D., Ed.; VCH: Berlin, 1991; p 57.
(35) Toney, M. F.; Gordon, J. G.; Melroy, O. R. *SPIE Proc.* **1991**, *1550*, 140.
(36) Toney, M. F. In *Synchrotron Techniques in Interfacial Electrochemistry*; Melendres, C. A., Tadjeddine, A., Eds.; Kluwer: Dordrecht, 1994; p 109.
(37) Ocko, B. M.; Wang, J. In *Synchrotron Techniques in Interfacial Electrochemistry*; Melendres, C. A., Tadjeddine, A., Eds.; Kluwer: Dordrecht, 1994; p 127.
(38) Morita, S.; Okada, T.; Mikoshiba, N. *Jpn. J. Appl. Phys., Part 1* **1989**, *28*, 535−540.
(39) Trevor, D. J.; Chidsey, C. E. D.; Loiacono, D. N. *Phys. Rev. Lett.* **1989**, *62*, 929.

(40) Gao X. P.; Weaver M. J. *J. Electroanal. Chem.* **1994**, *367*, 259−264.
(41) Nichols, R. J.; Magnussen, O. M.; Hotlos, J.; Twomey, T.; Behm, R. J.; Kolb, D. M. *J. Electroanal. Chem. Interfacial Electrochem.* **1990**, *290*, 21−31.
(42) Batina, N.; Dakkouri, A. S.; Kolb, D. M. *J. Electroanal. Chem.* **1994**, *370*, 87−94.
(43) Breuer, N.; Stimming, U.; Vogel, R. *Surf. Coat. Technol.* **1994**, *67*, 145−149.
(44) Ikemiya, N.; Nishide, M.; Hara, S. *Surf. Sci.* **1995**, *340*, L965−L970.
(45) Itaya, K.; Higaki, K.; Sugawara, S. *Chem. Lett.* **1988**, 421−424.
(46) Uosaki, K; Kita, H *J. Vac. Sci. Technol., A* **1990**, *8*, 520−524.
(47) Szklarczyk, M.; Bockris, J. O. *Surf. Sci.* **1991**, *241*, 54−60.
(48) Sashikata, K.; Furuya, N.; Itaya, K. *J. Vac. Sci. Technol., B* **1991**, *9*, 457−464.
(49) Vogel, R.; Kamphausen, I.; Baltruschat, H. *Ber. Bunsen-Ges. Phys. Chem.* **1992**, *96*, 525−530.
(50) Wan, L. J.; Yau, S. L.; Swain, G. M.; Itaya, K. *J. Electroanal. Chem.* **1995**, *381*, 105−111.
(51) Soriaga, M. P.; Schimpf, J. A.; Carrasquillo, A., Jr.; Abreu, J. B.; Temesghen, W.; Barriga, R. J.; Jeng, J.-J.; Sashikata, K.; Itaya, K. *Surf. Sci.* **1995**, *335*, 273−280.
(52) Christoph, R.; Siegenthaler, H.; Rohrer, H.; Wiese, H. *Electrochim. Acta* **1989**, *34*, 1011−1022.
(53) Hoepfner, M.; Obretenov, W.; Juettner, K.; Lorenz, W. J.; Staikov, G.; Bostanov, V.; Budevski, E. *Surf. Sci.* **1991**, *248*, 225−233.
(54) Dietterle, M.; Will, T.; Kolb, D. M. *Surf. Sci.* **1995**, *327*, L495−L500.
(55) Wolf, J. F.; Vicenzi, B.; Ibach, H. *Surf. Sci.* **1991**, *249*, 233.
(56) Poensgen, M.; Wolf, J. F.; Frohn, J.; Giesen, M.; Ibach, H. *Surf. Sci.* **1992**, *274*, 430.
(57) Giesen-Siebert, M.; Ibach, H. *Surf. Sci.* **1994**, *316*, 205.
(58) Cruickshank, B. J.; Sneddon, D. D.; Gewirth, A. A. *Surf. Sci.* **1993**, *281*, L308−L314.
(59) Suggs, W.; Bard, A. J. *J. Am. Chem. Soc.* **1994**, *116*, 10725.
(60) LaGraff, J. R.; Gewirth, A. A. *Surf. Sci.* **1995**, *326*, L461−L466.
(61) Ikemiya, N.; Kubo, T.; Hara, S. *Surf. Sci.* **1995**, *323*, 81−90.
(62) Lev, O.; Fan, F. R.; Bard, A. J. *J. Electrochem. Soc.* **1988**, *135*, 783−784.
(63) Chen, R. R.; Mo Y. B.; Scherson, D. A. *Langmuir* **1994**, *10*, 3933−3936.
(64) Suzuki, T.; Yamada, T.; Itaya, K. *J. Phys. Chem.* **1996**, *100*, 8954−8961.
(65) Kolb, D. M. *Prog. Surf. Sci.* **1996**, *51*, 109−173.
(66) Kolb, D. M.; Schneider, J. *Electrochim. Acta* **1986**, *31*, 929−936.
(67) Hamelin, A. *J. Electroanal. Chem.* **1988**, *255*, 281−289.
(68) Gao, X.; Hamelin, A.; Weaver, M. J. *Phys. Rev. Lett.* **1991**, *67*, 618−621.
(69) Hamelin, A.; Gao, X.; Weaver, M. J. *J. Electroanal. Chem.* **1992**, *323*, 361−367.
(70) Hamelin A.; Stoicoviciu L.; Edens G. J.; Gao X. P.; Weaver M. J. *J. Electroanal. Chem.* **1994**, *365*, 47−57.
(71) Gao, X.; Edens, G. J.; Hamelin, A.; Weaver, M. J. *Surf. Sci.* **1993**, *296*, 333−351.
(72) Magnussen, O. M.; Hotlos, J.; Behm, R. J.; Batina, N.; Kolb, D. M. *Surf. Sci.* **1993**, *296*, 310−332.
(73) Tao, N. J.; Lindsay, S. M. *J. Appl. Phys.* **1991**, *70*, 5141−5143.
(74) Gao, X.; Hamelin, A.; Weaver, M. J. *J. Chem. Phys.* **1991**, *95*, 6993−6996.
(75) Gao, X. P.; Edens, G. J.; Hamelin, A.; Weaver, M. J. *Surf. Sci.* **1994**, *318*, 1−20.
(76) Magnussen, O. M.; Wiechers, J.; Behm, R. J. *Surf. Sci.* **1993**, *289*, 139−151.
(77) Haiss, W.; Sass, J. K. *J. Electroanal. Chem.* **1995**, *386*, 267−270.
(78) Edens, G. J.; Gao, X. P.; Weaver, M. J.; Markovic, N. M.; Ross, P. N. *Surf. Sci.* **1994**, *302*, L275−L282.
(79) Gao, X.; Weaver, M. J. *Phys. Rev. Lett.* **1994**, *73*, 846−849.
(80) Gao, X.; Edens, G. J.; Weaver, M. J. *J. Phys. Chem.* **1994**, *98*, 8074−8085.
(81) Gao, X.; Weaver, M. J. *Surf. Sci.* **1994**, *313*, L775−L782.
(82) Zei, M. S.; Batina, N.; Kolb, D. M. *Surf. Sci.* **1994**, *306*, L519−L528.
(83) Villegas, I.; Weaver, M. J. *J. Electroanal. Chem.* **1994**, *373*, 245−249.
(84) Schardt, B. C.; Yau, S-L; Rinaldi, F. *Science* **1989**, *243*, 1050−1053.
(85) DeSimone, W. L.; Breen, J. J. *Langmuir* **1995**, *11*, 4428−4432.
(86) Tao, N. J.; Lindsay, S. M. *J. Phys. Chem.* **1992**, *96*, 5213−5217.
(87) Yamada T.; Batina N.; Itaya K. *Surf. Sci.* **1995**, *335*, 204−209.
(88) Yamada T.; Batina N.; Itaya K. *J. Phys. Chem.* **1995**, *99*, 8817−8823.
(89) Batina N.; Yamada T.; Itaya K. *Langmuir* **1995**, *11*, 4568−4576.
(90) Nagatani, Y.; Hayashi, T.; Yamada, T.; Itaya, K. *Jpn. J. Appl. Phys. Pt. 1* **1996**, *35*, 720−728.
(91) Tanaka, S.; Yau, S. L:.; Itaya, K. *J. Electroanal. Chem.* **1995**, *396*, 125−130.
(92) Schott, J. H.; White, H. S. *J. Phys. Chem.* **1994**, *98*, 291−296.
(93) Schott, J. H.; White, H. S. *Langmuir* **1994**, *10*, 486−491.
(94) Schott, J. H.; White, H. S. *J. Phys. Chem.* **1994**, *98*, 297−302.
(95) Sneddon, D. D.; Gewirth, A. A. *Surf. Sci.* **1995**, *343*, 185−200.
(96) Stuhlmann, C.; Villegas, I.; Weaver, M. J. *Chem. Phys. Lett.* **1994**, *219*, 319−324.
(97) Kim, Y. G.; Yau, S. L.; Itaya, K. *J. Am. Chem. Soc.* **1996**, *118*, 393−400.
(98) Sawaguchi, T.; Yamada, T.; Okinaka, Y.; Itaya, K. *J. Phys. Chem.* **1995**, *99*, 14149−14155.
(99) Gao, X.; Zhang, Y.; Weaver, M. J. *J. Phys. Chem.* **1992**, *96*, 4156−4159.
(100) Magnussen, O. M. *Faraday Disc.* **1992**, *94*, 399−400.
(101) Magnussen, O. M. Ph.D. Thesis; University of Ulm, 1993; pp 90−103.
(102) Edens, G. J.; Gao, X. P.; Weaver, M. J. *J. Electroanal. Chem.* **1994**, *375*, 357−366.
(103) Shi, S.; Lipkowski, M.; Gamboa, M.; Zelanay, P.; Wieckowski, A. *J. Electroanal. Chem.* **1994**, *366*, 373.
(104) Funtikov A. M.; Linke U.; Stimming U.; Vogel R. *Surf. Sci.* **1995**, *324*, L343−L348.
(105) Wan, L. J.; Yau, S. L.; Itaya, K. *J. Phys. Chem.* **1995**, *99*, 9507−9513.
(106) Kolb, D. M. In *Advances in Electrochemistry and Electrochemical Engineering*; Gerischer, H., Tobias, C. W., Eds.; Vol. 11; Wiley: New York, 1978; pp 125−271.
(107) Adzic, R. R. In *Advances in Electrochemistry and Electrochemical Engineering*; Gerischer, H., Tobias, C. W., Eds.; Vol. 13; Wiley-Interscience: New York, 1984; pp 159−260.
(108) Ikemiya, N.; Miyaoka, S.; Hara, S. *Surf. Sci.* **1994**, *311*, L641−L648.
(109) Hachiya, T.; Honbo, H.; Itaya, K. *J. Electroanal. Chem. Interfacial Electrochem.* **1991**, *315*, 275−291.
(110) Hölzle, M. H.; Kolb, D. M. *Ber. Bunsen-Ges. Phys. Chem.* **1994**, *98*, 330−335.
(111) Hölzle, M. H.; Zwing, V.; Kolb, D. M. *Electrochim. Acta* **1995**, *40*, 1237−1247.
(112) Sun, L.; Crooks, R. M. *J. Electrochem. Soc.* **1991**, *138*, L23−L25.
(113) Abe, T.; Miki, Y.; Itaya, K. *Bull. Chem. Soc. Jpn.* **1994**, *67*, 2075−2078.
(114) Shi, Z.; Lipkowski, J. *J. Electroanal. Chem.* **1994**, *365*, 303−309.
(115) Toney, M. F.; Howard, J. N.; Richer, J.; Borges, G. L.; Gordon, J. G.; Melroy, O. R.; Dennis, Y.; Sorensen, L. B. *Phys. Rev. Lett.* **1995**, *75*, 4472−4475.
(116) Huckaby, D. A.; Blum, L. *J. Electroanal. Chem.* **1991**, *315*, 255.
(117) Batina, N.; Will, T.; Kolb, D. M. *Faraday Disc.* **1992**, *94*, 93−106.
(118) Hotlos, J.; Magnussen, O. M.; Behm, R. J. *Surf. Sci.* **1995**, *335*, 129−144.
(119) Möller, F.; Magnussen, O. M.; Behm, R. J. *Phys. Rev. B* **1995**, *51*, 2484−2490.
(120) Möller, F.; Magnussen, O. M.; Behm, R. J. *Electrochim. Acta* **1995**, *40*, 1259−1265.
(121) Ikemiya, N.; Miyaoka, S.; Hara, S. *Surf. Sci.* **1995**, *327*, 261−273.
(122) Chen, C.-h.; Vesecky, S. M.; Gewirth, A. A. *J. Am. Chem. Soc.* **1992**, *114*, 451−458.
(123) Hachiya, T.; Itaya, K. *Ultramicroscopy* **1992**, *42−44*, 445−452.
(124) Ogaki, K.; Itaya, K. *Electrochim. Acta* **1995**, *40*, 1249−1257.
(125) Mrozek, P.; Sung, Y.; Han, M.; Gamboa-Aldeco, M.; Wieckowski, A.; Chen, C.-h.; Gewirth, A. A. *Electrochim. Acta* **1995**, *40*, 17−28.
(126) Corcoran, S. Q.; Chakarova, G. S.; Sieradzki, K. *J. Electroanal. Chem.* **1994**, *377*, 85−90.
(127) Ikemiya, N.; Yamada, K.; Hara, S. *Surf. Sci.* **1996**, *348*, 253−260.
(128) Staikov, G.; Juettner, K.; Lorenz, W. J.; Budevski, E. *Electrochim. Acta* **1994**, *39*, 1019−1029.
(129) Garcia, S. G.; Salinas, D.; Mayer, C.; Vilche, J. R.; Pauling, H.-J.; Vinzelberg, S.; Staikov, G.; Lorenz, W. J. *Surf. Sci.* **1994**, *316*, 143−156.
(130) Hamelin, A. *J. Electroanal. Chem.* **1979**, *101*, 285−290.
(131) Jüttner, K. *Electrochim. Acta* **1984**, *29*, 1597−1604.
(132) Green, M. P.; Richter, M.; Xing, X.; Scherson, D.; Hanson, K. J.; Ross, P. N., Jr.; Carr, R.; Lindau, I. *J. Microsc.* **1988**, *152*, 823−829.
(133) Green, M. P.; Hanson, K. J.; Scherson, D. A.; Xing, X.; Richter, M.; Ross, P. N.; Carr, R.; Lindau, I. *J. Phys. Chem.* **1989**, *93*, 2181−2184.
(134) Green, M. P.; Hanson, K. J.; Carr, R.; Lindau, I. *J. Electrochem. Soc.* **1990**, *137*, 3493−3498.
(135) Tao, N. J.; Pan, J.; Li, Y.; Oden, P. I.; DeRose, J. A.; Lindsay, S. M. *Surf. Sci.* **1992**, *271*, L388−L344.
(136) Chen, C.-h.; Washburn, N.; Gewirth, A. A. *J. Phys. Chem.* **1993**, *97*, 9754−9760.
(137) Sayed, S. M.; Jüttner, K. *Electrochim. Acta* **1983**, *28*, 1635−1641.
(138) Chen, C.-h. C.; Gewirth, A. A. *J. Am. Chem. Soc.* **1992**, *114*, 5439−5440.

(139) Chen, C.-h.; Kepler, K. D.; Gewirth, A. A.; Ocko, B. M.; Wang, J. *J. Phys. Chem.* **1993**, *97*, 7290−7294.
(140) Polewska, W.; Wang, J. X.; Ocko, B. M.; Adzic, R. R. *J. Electroanal. Chem.* **1994**, *376*, 41−47.
(141) Bondos, J. C.; Gewirth, A. A.; Nuzzo, R. G. *J. Phys. Chem.* **1996**, *100*, 8617−8620.
(142) Chen, C.-h.; Gewirth, A. A. *Phys. Rev. Lett.* **1992**, *68*, 1571−1574.
(143) Inukai, J.; Sugita, S.; Itaya, K. *J. Electroanal. Chem.* **1996**, *403*, 159−168.
(144) Lorenz, W. J.; Gassa, L. M.; Schmidt, U.; Obretenov, W.; Staikov, G.; Bostanov, V.; Budevski, E. *Electrochim. Acta* **1992**, *37*, 2173.
(145) Obretenov, W.; Schmidt, U.; Lorenz, W. J.; Staikov, G.; Budevski, E.; Carnal, D.; Mueller, U.; Siegenthaler, H.; Schmidt, E. *Faraday Disc.* **1992**, *94*, 107−116.
(146) Obretenov, W.; Schmidt, U.; Lorenz, W. J.; Staikov, G.; Budevski, E.; Carnal, D.; Mueller, U.; Siegenthaler, H.; Schmidt, E. *J. Electrochem. Soc.* **1993**, *140*, 692−703.
(147) Carnal, D.; Oden, P. I.; Mueller, U.; Schmidt, E.; Siegenthaler, H. *Electrochim. Acta* **1995**, *40*, 1223−1235.
(148) Staikov, G.; Juettner, K.; Lorenz, W. J.; Budevski, E. *Electrochim. Acta* **1994**, *39*, 1019−1029.
(149) Pauling, H. J.; Juettner, K. *Electrochim. Acta* **1992**, *37*, 2237−2244.
(150) Jüttner, K.; Pauling, H. J. *Bull. Electrochem.* **1992**, *8*, 62−69.
(151) Suggs, D. W.; Stickney, J. L. *Surf. Sci.* **1993**, *290*, 375−387.
(152) Sashikata, K.; Furuya, N.; Itaya, K. *J. Electroanal. Chem.* **1991**, *316*, 361−368.
(153) Shingaya, Y.; Matsumoto, H.; Ogasawara, H.; Ito, M. *Surf. Sci.* **1995**, *335*, 23−31.
(154) Abe, T.; Swain, G. M.; Sashikata, K.; Itaya, K. *J. Electroanal. Chem.* **1995**, *382*, 73−83.
(155) Beitel, G.; Magnussen, O. M.; Behm, R. J. *Surf. Sci.* **1995**, *336*, 19−26.
(156) Wuensche, M.; Nichols, R. J.; Schumacher, R.; Beckmann, W.; Meyer, H. *Electrochim. Acta* **1993**, *38*, 647−652.
(157) Shinotsuka, N.; Sashikata, K.; Itaya, K. *Surf. Sci.* **1995**, *335*, 75−82.
(158) Matsumoto, H.; Inukai, J.; Ito, M. *J. Electroanal. Chem.* **1994**, *379*, 223−231.
(159) Adzic, R. R.; Wang, J.; Vitus, C. M.; Ocko, B. M. *Surf. Sci.* **1993**, *293*, L876−L883.
(160) Oda, I.; Shingaya, Y.; Matsumoto, H.; Ito, M. *J. Electroanal. Chem.* **1996**, *409*, 95−101.
(161) Ge, M.; Gewirth, A. A. *Surf. Sci.* **1994**, *324*, 140.
(162) Armstrong, M. J.; Muller, R. H. *J. Electrochem. Soc.* **1989**, *136*, 584−585.
(163) Uosaki, K; Kita, H. *J. Electroanal. Chem. Interfacial Electrochem.* **1989**, *259*, 301−308.
(164) Zhang, X.; Stimming, U. *J. Electroanal. Chem.* **1990**, *291*, 273.
(165) Zhang, X.; Stimming, U. *Corros. Sci.* **1990**, *30*, 951.
(166) Stimming, U.; Vogel, R.; Kolb, D. M.; Will, T. *J. Power Sources* **1993**, *43*, 169−180.
(167) Nichols, R. J.; Kolb, D. M.; Behm, R. J. *J. Electroanal. Chem. Interfacial Electrochem.* **1991**, *313*, 109−119.
(168) Ullmann, R.; Will, T.; Kolb, D. M. *Ber. Bunsen-Ges. Phys. Chem.* **1995**, *99*, 1414−20.
(169) Ullmann, R.; Will, T.; Kolb, D. M. *Chem. Phys. Lett.* **1993**, *209*, 238−242.
(170) Batina, N.; Will, T.; Kolb, D. M. *Faraday Disc.* **1992**, *94*, 93−106.
(171) Batina, N.; Kolb, D. M.; Nichols, R. J. *Langmuir* **1992**, *8*, 2572−2576.
(172) Nichols, R. J.; Beckmann, W.; Meyer, H.; Batina, N.; Kolb, D. M. *J. Electroanal. Chem.* **1992**, *330*, 381−394.
(173) Nichols, R. J.; Bach, C. E.; Meyer, H. *Ber. Bunsen-Ges. Phys. Chem.* **1993**, *97*, 1012.
(174) Nichols, R. J.; Bunge, E.; Meyer, H.; Baumgartel, H. *Ber. Bunsen-Ges. Phys. Chem.* **1995**, *99*, 1243−1246.
(175) Rynders, R. M.; Alkire, R. C. *J. Electrochem. Soc.* **1994**, *141*, 1166−1173.
(176) Will, T.; Dietterle, M.; Kolb, D. M. In *Nanoscale Probes of the Solid/Liquid Interface*; Gewirth, A. A., Siegenthaler, H., Eds.; NATO ASI Series E; Kluwer Academic: Dordrecht, 1995; Vol. 288, 137−162.
(177) Josefowicz, J. Y.; Xie, L.; Farrington, G. C. *J. Phys. Chem.* **1993**, *97*, 11995−11998.
(178) Srinivasan, R.; Gopalan, P. *Surf. Sci.* **1995**, *338*, 31−40.
(179) Andersen, J.; Bech-Nielsen, G.; Moeller, P.; Reeve, J. C. *J. Appl. Electrochem.* **1996**, *26*, 161−170.
(180) Andersen, J.; Moeller, P *J. Electrochem. Soc.* **1995**, *142*, 2225−2232.
(181) Schmidt, W. U.; Alkire, R. C. *J. Electrochem. Soc.* **1994**, *141*, L85−L87.
(182) Andersen, J.; Bech-Nielsen, G.; Möller, P. *Surf. Coat. Technol.* **1994**, *67*, 151−159.
(183) Sondag-Huethorst, J. A. M.; Fokkink, L. G. J. *Langmuir* **1995**, *11*, 4823−4831.
(184) Eliadis, E. D.; Nuzzo, R. G.; Gewirth, A. A.; Alkire, R. C. *J. Electrochem. Soc.* **1997**, *144*, 96−105.
(185) Dietterle, M.; Will, T.; Kolb, D. M. *Surf. Sci.* **1995**, *342*, 29−37.
(186) Schröer, D.; Nichols, R. J.; Meyer, H. *Electrochim. Acta* **1995**, *40*, 1487−1494.
(187) Nichols, R. J.; Schröer, D.; Meyer, H. *Electrochim. Acta* **1995**, *40*, 1479−1486.
(188) Iwaski, H.; Yoshinobu, T. *Phys. Rev. B* **1993**, *48*, 8282.
(189) Schmidt, W. U.; Alkire, R. C.; Gewirth, A. A. *J. Electrochem. Soc.* **1996**, *143*, 3122−3132.
(190) Sonnenfeld, R.; Schardt, B. C. *Appl. Phys. Lett.* **1986**, *49*, 1172.
(191) Robinson, R. S. *J. Vac. Sci. Technol., A* **1990**, *8*, 511−514.
(192) Kowal, K.; Xie, L.; Huq, R.; Farrington, G. C. *J. Electrochem. Soc.* **1994**, *141*, 116−122.
(193) Yoon, B. U.; Cho, K.; Kim, H. *Anal. Sci.* **1996**, *12*, 321−326.
(194) Poetzschke, R. T.; Gervasi, C. A.; Vinzelberg, S.; Staikov, G.; Lorenz, W. J. *Electrochim. Acta* **1995**, *40*, 1469−1474.
(195) Li, W.; Virtanen, J. A.; Penner, R. M. *J. Phys. Chem.* **1992**, *96*, 6529−6532.
(196) Li, W.; Hsiao, G. S.; Harris, D.; Nyffenegger, R. M.; Virtanen, J. A.; Penner, R. M. *J. Phys. Chem.* **1996**, *100*, 20103−20113.
(197) Zoval, J. V.; Stiger, R. M.; Biernacki, P. R.; Penner, R. M. *J. Phys. Chem.* **1996**, *100*, 837−844.
(198) Van der Eerden, J. P.; Mickers, M. A. H.; Gerritsen, J. W.; Hottenhuis, M. H. J. *Electrochim. Acta* **1989**, *34*, 1141−1145.
(199) Wichman, B.; Van der Eerden, J. P.; Gerritsen, J. W. *J. Cryst. Growth* **1990**, *99*, 1333−1338.
(200) Endo, K.; Sugawara, Y.; Mishima, S.; Okada, T.; Morita, S. *Jpn. J. Appl. Phys., Part 1* **1991**, *30*, 2592−2593.
(201) Lorenz, W. J.; Staikov, G. *Surf. Sci.* **1995**, *335*, 32−43.
(202) Staikov, G.; Juettner, K.; Lorenz, W. J.; Budevski, E. *Electrochim. Acta* **1994**, *39*, 1019−1029.
(203) Garcia, S. G.; Salinas, D.; Mayer, C.; Vilche, J. R.; Pauling, H.-J.; Vinzelberg, S.; Staikov, G.; Lorenz, W. J. *Surf. Sci.* **1994**, *316*, 143−156.
(204) Sugita, S.; Abe, T.; Itaya, K. *J. Phys. Chem.* **1993**, *97*, 8780.
(205) Hachiya, T.; Itaya, K. *Ultramicroscopy* **1992**, *42*−44, 445−452.
(206) Corcoran, S. G.; Chakarova, G. S.; Sieradzki, K. *Phys. Rev. Lett.* **1993**, *71*, 1585.
(207) Ikemiya, N.; Yamada, K.; Hara, S. *J. Vac. Sci. Technol. B* **1996**, *14*, 1369−1372.
(208) Kolb, D. M. Presented at the 1996 National Meeting of the Materials Research Society, Boston, MA, 1996.
(209) Chen, Z.; Li, J.; Wang, E. *J. Electroanal. Chem.* **1994**, *373*, 83−87.
(210) Homma, T.; Yamazaki, T.; Osaka, T. *J. Electrochem. Soc.* **1992**, *139*, 732−736.
(211) Tong, X. Q.; Aindow, M.; Farr, J. P. G. *J. Electroanal. Chem.* **1995**, *395*, 117−126.
(212) Tong, X. Q.; Aindow, M.; Farr, J. P. G. *Microsc. Res. Tech.* **1996**, *34*, 87−95.
(213) Nishitani, R.; Kasuya, A.; Nishina, Y. *Z. Phys. D: At. Mol. Clusters* **1993**, *26*, 42−44.
(214) Shaikhutdinov, S. K.; Möller, F. A.; Mestl, G.; Behm, R. J. *J. Catal.* **1996**, *163*, 492−495.
(215) Möller, F. A.; Magnussen, O. M.; Behm, R. J. *Phys. Rev. Lett.* **1996**, *77*, 5249−5252.
(216) Möller, F. A.; Magnussen, O. M.; Behm, R. J. *Phys. Rev. Lett.* **1996**, *77*, 3165−3168.
(217) Yang, X. M.; Tonami, K.; Nagahara, L. A.; Hashimoto, K.; Wei, Y.; Fujishima, A. *Surf. Sci.* **1994**, *319*, L17−L22.
(218) Yang, X.; Tonami, K.; Nagahara, L. A.; Hashimoto, K.; Wei, Y.; Fujishima, A. *Chem. Lett.* **1994**, 2059−2062.
(219) Baldauf, M.; Kolb, D. M. *Electrochim. Acta* **1993**, *38*, 2145−2153.
(220) Moffat, T. P.; Fan, F. R. F.; Bard, A. J. *J. Electrochem. Soc.* **1991**, *138*, 3224−3235.
(221) Pickering, H. W.; Wo, T. C.; Gregory D. S.; Geh, S.; Sakurai *J. Vac. Sci. Technol. B* **1991**, *9*, 976−983.
(222) Breuer, N.; Stimming, U.; Vogel, R. *Electrochim. Acta* **1995**, *40*, 1401−1409.
(223) Josefowicz, J. Y.; Xie, L.; Farrington, G. C. *J. Phys. Chem.* **1993**, *97*, 11995−11998.
(224) Suggs, W.; Bard, A. J. *J. Am. Chem. Soc.* **1994**, *116*, 10725.
(225) Suggs, D. W.; Bard, A. J. *J. Phys. Chem.* **1995**, *99*, 8349−8355.
(226) Vogt, M. R.; Möller, F. A.; Schilz, C. M.; Magnussen, O. M.; Behm, R. J. *Surf. Sci.* **1996**, *367*, L33−L41.
(227) Cruickshank, B. J.; Gewirth, A. A.; Rynders, R. M.; Alkire, R. C. *J. Electrochem. Soc.* **1992**, *139*, 2829−2832.
(228) Fan, F. R. F.; Bard, A. J. *J. Electrochem. Soc.* **1989**, *136*, 166−170.
(229) Miyasaka, A.; Ogawa, H. *Corros. Sci.* **1990**, *31*, 99−104.
(230) Ryan, M. P.; Newman, R. C.; Fujimoto, S.; Thompson, G. E.; Corcoran, S. G.; Sieradski, K. In *Modifications of Passive Films*; Marcus, P., Baroux, B., Keddam, M., Eds.; Institute of Materials: London, 1993; p 66.
(231) Ryan, M. P.; Newman, R. C.; Thompson, G. E. *J. Electrochem. Soc.* **1994**, *141*, L164−L165.
(232) Bhardwaj, R. C.; Gonzalez-Martin, A.; Bockris, J. O. *J. Electrochem. Soc.* **1991**, *138*, 1901−1908.
(233) Ryan, M. P.; Newman, R. C.; Thompson, G. E. *J. Electrochem. Soc.* **1995**, *142*, L177−L179.

(234) Walls, M. Q.; Ponthieux, A.; Rondot, B.; Owen, R. A. *J. Vac. Sci. Technol. A* **1996**, *14*, 1362−1367.
(235) Bhardwaj, R. C.; Gonzalez-Martin, A.; Bockris, J. O. *J. Electroanal. Chem. Interfacial Electrochem.* **1991**, *307*, 195−207.
(236) Bhardwaj, R. C.; Gonzalez-Martin, A.; Bockris, J. O. *J. Electrochem. Soc.* **1992**, *139*, 1050−1058.
(237) Chen, L.; Guay, D. *J. Electrochem. Soc.* **1994**, *141*, L43−L45.
(238) Chen, L.; Guay, D. *Langmuir* **1996**, *12*, 5818−5823.
(239) Oppenheim, I. C.; Trevor, D. J.; Chidsey, C. E. D. *Science* **1991**, *254*, 687.
(240) Li, Y.-Q.; Chailapakul, O.; Crooks, R. M. *J. Vac. Sci. Technol. B* **1995**, *13*, 1300−1306.
(241) Ando, S.; Suzuki, T.; Itaya, K. *J. Electroanal. Chem.* **1996**, *412*, 139−146.
(242) Sashikata, K.; Matsui, Y.; Itaya, K.; Soriaga, M. P. *J. Phys. Chem.* **1996**, *100*, 20027−20034.
(243) Goss, C. A.; Brumfield, J. C.; Irene, E. A.; Murray, R. W. *Anal. Chem.* **1993**, *65*, 1378.
(244) Hathcock, K. W.; Brumfield, J. C.; Goss C. A.; Irene, E. A.; Murray, R. W. *Anal. Chem.* **1995**, *67*, 2201−2206.
(245) Wang, J.; Martinez, T.; Yaniv, D. R.; McCormick, L. D. *J. Electroanal. Chem. Interfacial Electrochem.* **1990**, *278*, 379−386.
(246) Allongue, P. In *Nanoscale Probes of the Solid/Liquid Interface*; Gewirth, A. A., Siegenthaler, H., Eds.; NATO ASI Series E; Kluwer Academic: Dordrecht, 1995; Vol. 288, 45−67.
(247) Itaya, K.; Tomita E. *Chem. Lett.* **1989**, 285−289.
(248) Itaya, K.; Tomita, E. *Surf. Sci.* **1989**, *219*, L515−L520.
(249) Eriksson, S.; Carlsson, P.; Holmstroem, B.; Uosaki, K. *J. Electroanal. Chem. Interfacial Electrochem.* **1991**, *313*, 121−128.
(250) Koinuma, M.; Uosaki, K. *J. Vac. Sci. Technol. B* **1994**, *12*, 1543−1546.
(251) Koinuma, M.; Uosaki, K. *Surf. Sci.* **1994**, *311*, L737−L742.
(252) Uosaki, K.; Koinuma, M. *Sol. Energy Mater. Sol. Cells* **1995**, *38*, 347−348.
(253) Yao, H.; Yau, S. L.; Itaya, K. *Surf. Sci.* **1995**, *335*, 166−170.
(254) Yau, H.; Yau, S. L.; Itaya, K. *Appl. Phys. Lett.* **1996**, *68*, 1473−1475.
(255) Eriksson, S.; Carlsson, P.; Holmstroem, B.; Uosaki, K. *J. Electroanal. Chem.* **1992**, *337*, 217−227.
(256) Koinuma, M.; Uosaki, K. *Surf. Sci.* **1996**, *358*, 565−570.
(257) Szklarczyk, M.; Gonzalez-Martin, A.; Bockris, J. O. *Surf. Sci.* **1991**, *257*, 307−318.
(258) Allongue, P.; Brune, H.; Gerischer, H. *Surf. Sci.* **1992**, *275*, 414−423.
(259) Kaji, K.; Yau, S. L.; Itaya, K. *J. Appl. Phys.* **1995**, *78*, 5727−5733.
(260) Yau, S. L. Kaji, K. Itaya, K. *Appl. Phys. Lett.* **1995**, *66*, 766−768.
(261) Ye, J. H.; Kaji, K.; Itaya, K. *J. Electrochem. Soc.* **1996**, *143*, 4012−4019.
(262) Yoshihara, S.; Endo, K.; Sato, E.; Bockris, J. O. *J. Electroanal. Chem.* **1994**, *372*, 91−94.
(263) Zhao, X. K.; McCormick, L.; Fendler, J. H. *Chem. Mater.* **1991**, *3*, 922−935.
(264) Demir, U.; Shannon, C. *Langmuir* **1994**, *10*, 2794−2799.
(265) Sakamaki, K.; Hinokuma, K.; Hashimoto, K.; Fujishima, A. *Surf. Sci.* **1990**, *237*, L383−L389.
(266) Sakamaki, K.; Hinokuma, K.; Fujishima, A. *Collect. Czech. Chem. Commun.* **1991**, *56*, 104−111.
(267) Higgins, S. R.; Hamers, R. J. *Surf. Sci.* **1995**, *324*, 263−281.
(268) Higgins, S. R.; Hamers, R. J. *J. Vac. Sci. Technol. B* **1996**, *14*, 1360−1364.
(269) Uosaki, K; Kita, H. *J. Electroanal. Chem. Interfacial Electrochem.* **1989**, *259*, 301−308.
(270) Homma, T.; Yamazaki, T.; Kubota, T.; Osaka, T. *Jpn. J. Appl. Phys.* **1990**, *29*, L2114−L2117.
(271) Wouters, G.; Bratoeva, M.; Celis, J.-P.; Roos, J. R. *Electrochim. Acta* **1995**, *40*, 1439−1453.
(272) Dubois, L.; Nuzzo, R. G. *Annu. Rev. Phys. Chem.* **1992**, *43*, 437−463.
(273) Pan, J.; Tao, N. J.; Lindsay, S. M. *Langmuir* **1993**, *9*, 1556−1560.
(274) Dakkouri, A. S.; Kolb, D. M.; Edelstein-Shima, R.; Mandler, D. *Langmuir* **1996**, *12*, 2849−2852.
(275) Han, W.; Li, S.; Lindsay, S. M.; Gust, D.; Moore, T. A.; Moore, A. L. *Langmuir* **1996**, *12*, 5742.
(276) Li, W. J.; Virtanen, J. A.; Penner, R. M. *J. Phys. Chem.* **1994**, *98*, 11751−11755.
(277) Oda, I.; Inukai, J.; Ito, M. *Chem. Phys. Lett.* **1993**, *203*, 99−103.
(278) Villegas, I.; Weaver, M. J. *J. Chem. Phys.* **1994**, *101*, 1648−1660.
(279) Vitus, C. M.; Chang, S.; Schardt, B. C.; Weaver, M. J. *J. Phys. Chem.* **1991**, *95*, 7559−7563
(280) Villegas, I.; Gao, X. P.; Weaver, M. J. *Electrochim. Acta* **1995**, *40*, 1267−1275.
(281) Yau, S. L.; Gao, X. P.; Chang, S. C.; Schardt, B. C.; Weaver, M. J. *J. Am. Chem. Soc.* **1991**, *113*, 6049−6056.
(282) Gao, X. P.; Chang, S.; Jiang, X.; Hamelin, A.; Weaver, M. J. *J. Vac. Sci. Technol. A* **1992**, *10*, 2972−2980.
(283) Srinivasan, R.; Murphy, J. C. *Ultramicroscopy* **1992**, *42*, 453−459.
(284) Srinivasan, R.; Murphy, J. C.; Fainchtein, R. *J. Electroanal. Chem.* **1991**, *312*, 293.
(285) Lindsay, S. M.; Tao, N. J.; DeRose, J. A.; Oden, P. I.; Lyubchenko, Y. L.; Harrington, R. E.; Shlyakhtenko, L. *Biophys. J.* **1992**, *61*, 1570.
(286) Tao, N. J.; DeRose, J. A.; Lindsay, S. M. *J. Phys. Chem.* **1993**, *97*, 910.
(287) Tao, N. J.; Shi, Z. *J. Phys. Chem.* **1994**, *98*, 1464−1471.
(288) Wang, X. W.; Tao, N. J.; Cunha, F. *J. Chem. Phys.* **1996**, *105*, 3747−3752.
(289) Tao, N. J.; Shi, Z. *J. Phys. Chem.* **1994**, *98*, 7422−7426.
(290) Tao, N. J.; Shi, Z. *Surf. Sci.* **1994**, *321*, L149−L156.
(291) Cunha, F.; Tao, N. J. *Phys. Rev. Lett.* **1995**, *75*, 2376−2379.
(292) Hölzle, M. H.; Krznaric, D.; Kolb, D. M. *J. Electroanal. Chem.* **1995**, *386*, 235−239.
(293) Wandlowski, T.; Lampner, D.; Lindsay, S. M. *J. Electroanal. Chem.* **1996**, *404*, 215−226.
(294) Hölzle, M. H.; Wandlowski, T.; Kolb, D. M. *Surf. Sci.* **1995**, *335*, 281−290.
(295) Hölzle, M. H.; Wandlowski, T.; Kolb, D. M. *J. Electroanal. Chem.* **1995**, *394*, 271−275.
(296) Bunge, E.; Nichols, R. J.; Roelfs, B.; Meyer, H.; Buamgartel, H. *Langmuir* **1996**, *12*, 3060
(297) Richard, K. M.; Gewirth, A. A. *J. Phys. Chem.* **1995**, *99*, 12288−12293.
(298) Richard, K. M.; Gewirth, A. A. *J. Electrochem. Soc.* **1996**, *143*, 2088−2092.
(299) Richard, K. M.; Gewirth, A. A. *J. Phys. Chem.* **1996**, *100*, 7204−7211.
(300) Wang, J.; Martinez, T.; Daphna, R. Y.; McCormick, L. D. *J. Electroanal. Chem.* **1991**, *313*, 129−140.
(301) Sasano, K.; Nakamura, K.; Kaneto, K. *Jpn. J. Appl. Phys., Part 2* **1993**, *32*, L863−L865.
(302) Nyffenegger, R. M.; Penner, R. M. *J. Phys. Chem.* **1996**, *100*, 17041−17049.
(303) Chao, F.; Costa, M.; Tian, C. *Analysis* **1994**, *22*, M32−M34.
(304) Tao, N. J.; Cardenas, G.; Cunha, F.; Shi, Z. *Langmuir* **1995**, *11*, 4445−4448.
(305) Tao, N. J. *Phys. Rev. Lett.* **1996**, *76*, 4066−4069.
(306) Kunitake, M.; Batina, N.; Itaya, K. *Langmuir* **1995**, *11*, 2337−2340.
(307) Ogaki, K.; Batina, N.; Kunitake, M.; Itaya, K. *J. Phys. Chem.* **1996**, *100*, 7185−7190.
(308) Batina, N.; Kunitake, M.; Itaya, K. *J. Electroanal. Chem.* **1996**, *405*, 245.
(309) Ohtani, H.; Wilson, R. J.; Chiang, S.; Mate, C. M. *Phys. Rev. Lett.* **1988**, *60*, 2398.
(310) Yau, S. L.; Kim, Y. G.; Itaya, K. *J. Am. Chem. Soc.* **1996**, *118*, 7795−7803.
(311) Ge, M.; Zhong, B.; Klemperer, W. G.; Gewirth, A. A. *J. Am. Chem. Soc.* **1996**, *118*, 5812−5813.

CR960067Y